The nature of the purine at position 34 in tRNAs of 4-codon boxes is correlated with nucleotides at positions 32 and 38 to maintain decoding fidelity

Ketty PERNOD[1], Laure SCHAEFFER[1], Johana CHICHER[2], Eveline HOK[3], Christian RICK[1], Renaud GESLAIN[3], Gilbert ERIANI[1], Eric WESTHOF[1], Michael RYCKELYNCK[1]*, Franck MARTIN[1]*

[1]Institut de Biologie Moléculaire et Cellulaire, "Architecture et Réactivité de l'ARN" CNRS UPR9002, Université de Strasbourg, 15, rue René Descartes, F-67084 Strasbourg (France)

[2]Institut de Biologie Moléculaire et Cellulaire, Plateforme Protéomique Strasbourg – Esplanade, CNRS FRC1589, Université de Strasbourg, 15, rue René Descartes, F-67084 Strasbourg (France)

[3]Laboratory of tRNA Biology, Department of Biology, Rita Liddy Hollings Science Center, 58 Coming Street, Charleston, South Carolina (USA)

*Corresponding authors

Emails for correspondence:
m.ryckelynck@unistra.fr or f.martin@ibmc-cnrs.unistra.fr

Keywords: IRES, translation, CrPV, ribosome, decoding, droplet-based microfluidics

ABSTRACT (199 words)

Translation fidelity relies essentially on the ability of ribosomes to accurately recognize triplet interactions between codons on mRNAs and anticodons of tRNAs. To determine the codon-anticodon pairs that are efficiently accepted by the eukaryotic ribosome, we took advantage of the IRES from the intergenic region (IGR) of the Cricket Paralysis Virus. It contains an essential pseudoknot PKI that structurally and functionally mimics a codon-anticodon helix. We screened the entire set of 4,096 possible combinations using ultrahigh-throughput screenings combining coupled transcription/translation and droplet-based microfluidics. Only 97 combinations are efficiently accepted and accommodated for translocation and further elongation: 38 combinations involve cognate recognition with Watson-Crick pairs and 59 involve near-cognate recognition pairs with at least one mismatch. More than half of the near-cognate combinations (36/59) contain a G at the first position of the anticodon (numbered 34 of tRNA). G34-containing tRNAs decoding 4-codon boxes are almost absent from eukaryotic genomes in contrast to bacterial genomes. We reconstructed these missing tRNAs and could demonstrate that these tRNAs are toxic to cells due to their miscoding capacity in eukaryotic translation systems. We also show that the nature of the purine at position 34 is correlated with the nucleotides present at 32 and 38.

INTRODUCTION

In the three kingdoms of life, translation of genetic information into proteins takes place on the macromolecular machine called the ribosome. Using messenger RNA as a template, the ribosome catalyses the sequential addition of amino acids to the nascent polypeptide chain by recruiting cognate aminoacylated tRNAs according to the successive codons. Cell integrity requires a high fidelity rate in order to avoid the production of potentially toxic aberrant proteins. Nevertheless, it has been estimated both in bacteria and eukaryotes that 18% of the proteins (from a 400-amino acid long protein) contain at least one mis-incorporated amino acid under normal physiological conditions (1). *E. coli* tolerates up to 10% of error-containing protein (2), while higher error rates, up to 50%, often lead to lethality by various mechanisms such as toxic protein production under stress conditions, for example, or protein misfolding (1, 3). In *E. coli*, errors due to incorrect tRNA aminoacylations occur rarely (4–7). Another source of errors is aberrant decoding, also called miscoding, on the ribosome itself. Such errors are caused by abnormal frameshifting (10^{-5} in prokaryotes) (8) or more frequently by missense errors when the ribosome accommodates a near-cognate aminoacylated tRNA on a codon (10^{-3}-10^{-4} both in *E.coli* and yeast) (1, 9–13). Structural investigations using X-ray crystallography with several near-cognate codon-anticodon pairs in the A site of the ribosome demonstrated that the ribosomal decoding grip can accommodate near-cognate tRNAs when pairing with the codon adopts a “Watson-Crick-like geometry” (14–17). After being accommodated in the ribosomal A site, the aminoacylated tRNA base-paired to the codon undergoes the translocation step that is defined by a concerted movement of the tRNA and the mRNA with respect to ribosomal subunits towards the P and later on the E sites (18, 19). Importantly, to avoid frameshifting, base pairing in the codon/anticodon helix is maintained during the whole translocation process (20). The low *in vivo* misreading rate suggests that the ribosome discriminates against most potential errors by preventing their translocation (10). Therefore, the miscoding rate results from the cumulative proofreading steps of (i) A-site accommodation of anticodon/codon duplex and (ii) translocation check point of the codon-anticodon mini helix prior movement from the A to the P site.

To gain further insights in decoding rules, we sought to identify all codon-anticodon combinations that are first efficiently accommodated in the A site and then further

allowed to undergo translocation to the P site. We used the Internal Ribosome Entry Site (IRES) from Cricket Paralysis Virus (CrPV). This dicistrovirus contains in its viral RNA genome two open reading frames separated by an InterGenic Region (IGR) IRES (21, 22). The IGR is able to promote translation initiation on any codon without the need of any translation initiation factor (eIF) or initiator tRNA (23–25). It folds into a sophisticated structure, which contains three pseudoknot structures PKI, PKII and PKIII (26). PK II and PKIII fold into compact domains that participate in ribosomal recruitment (27, 28). The IRES is properly positioned in the decoding centre of the ribosome by two other RNA domains, SLIV and SLV that directly interact with the small ribosomal subunit 40S (24, 29, 30). Most importantly, PKI functionally mimics a codon-anticodon helix and is recognized by the ribosome in the same way as a cognate mRNA-tRNA codon-anticodon duplex is (Figure 1 and S1) (30–32). Recent cryo-EM studies have demonstrated that PKI enters the ribosome by interacting with the A site in an identical manner as an aminoacylated tRNA base-paired to its cognate codon (30, 32). The IRES domains SLIV and SLV bind to the head of the ribosome, thereby restricting its flexibility, which allows the introduction of PKI in the A site (33). The same restriction of the ribosomal head movement is also observed during canonical translation (34, 35). Indeed, PKI accurately mimics structurally and functionally a tRNA anticodon base paired with the three nucleotides of the codon (Figure S1) (33). Moreover, biochemical experiments demonstrated that correct base pairing in PKI is a prerequisite for an active IGR IRES (36, 37). Once PKI is loaded into the A site, the elongation factor eEF-2 promotes further translocation of PKI toward the P site like the codon-anticodon mini helix during canonical translation (33, 38–40). When PKI is in the P site, contacts with SLIV and SLV are disrupted, leaving the A site free to accept the next aminoacylated tRNA and translation elongation of the native reporter protein can proceed (41). After translocation PKI dissociates in the E site and mimics the acceptor stem of an E-site tRNA (42).

Altogether, these studies confirmed that PKI follows the same path than a codon-anticodon duplex namely (i) discrimination of codon/anticodon duplex in the A site and (ii) its subsequent translocation from the A to the P site. However, unlike tRNAs, PKI does not contain any modified nucleotides that are known to influence codon-anticodon interactions. We used PKI as a molecular scaffold to investigate the functional constraints imposed by the ribosome decoding centre and identify in a

systematic fashion which codon/anticodon pairs of unmodified bases are able to support translation elongation. With an original approach that combines microfluidic technology with cell-free translation extracts, we could screen a library containing the 4,096 codon/anticodon combinations (64X64).

MATERIAL AND METHODS

Microfluidic-assisted ultrahigh-throughput screening procedure

Gene library preparation. IRES gene library with randomized codon/anticodon mimicking regions was prepared by PCR amplifying the CrPV IGR coding template using a sense primer (5'GTCGTCTAATCCAGAGACCCCGGATCGGATATTAATACGACTCACTATAGGC AAAAATGTGATCTTGCTT3') appending the T7 RNA polymerase promoter (underlined sequence) to the construct and an antisense primer (5'*CGAAGTATCTTGAAATGTAGC*NNNTAAATTTCTTAG-GTTTTTCGACTANNNAATCTGAAAAACCGCAGAGAGGGCTTCCTGG3') with the codon/anticodon mimicking regions randomized (symbolized by N in antisense primer sequence) with a controlled ratio of 25/25/25/25 for A/C/G/T (Integrated DNA Technologies). A PCR mixture containing 0.02 ng/µL of CrPV IGR-containing template plasmid, 0.2 µM of each primer (Integrated DNA Technologies), 0.2 mM of each dNTP (Thermofisher), 0.04 U/µL of Phusion DNA polymerase (Thermofisher) and the corresponding buffer at the recommended concentration was subjected to an initial denaturation step of 2 min at 95°C followed by 25 cycles of: 30 sec at 95°C, 30 sec at 55°C, 1 min at 72°C, and terminated by a final extension of 10 min at 72°C. The PCR product was then purified on a 1% agarose TBE gel, the band containing the product of interest was excised, the DNA recovered using a "Wizard® SV Gel and PCR Clean-Up System" kit (Promega) and quantified with a Nanodrop (Thermo Scientific). This PCR product was then used as primer in a second PCR reaction using as template the GFPMut2-containing plasmid (pGFP) we used in a previous study (43). This second PCR was performed in the same conditions as above but using 0.02 ng/µL of pGFP, 0.07 µM of the first PCR product (the region of the antisense primer complementary to GFP is italicized) and 0.2 µM of RevGFP primer (5' GAAGCGGCCGCTCTAGATTAATTTAAATC3'). Finally, this second PCR product was purified on a 1% agarose gel and quantified as above. The proper randomization of the library was confirmed by NGS analysis (Figure S2b). Importantly, even though some sequences were found slightly over-represented (dark blue combinations in the matrix), they did not introduce any bias in the selection process as they were not found in the enriched pools.

Droplet-based microfluidic screening. We used the same overall droplet-based microfluidics strategy we described before for the screening of ribozyme (44) or fluorogenic aptamer (45–47) gene libraries (Figure S2a) with a few adaptations.

i. Digital droplet PCR. First, DNA molecules were individualized into 2.5 pL PCR mixture-containing droplets by diluting the DNA solution such that only 1 out 10 droplets initially contained a DNA molecule to limit multiple encapsulation events. To do so, a PCR mixture containing 0.13 pM of template DNA diluted into 200 ng/µL yeast total RNA (Ambion), 0.2 µM of FwdIRES-GFP (5'GTCGTCTAATCCAGAGACCCCGGATCGG3') and RevGFP (5' GAAGCGGCCGCTCTAGATTAATTTAAATC3') primers, 0.2 mM of each dNTP (Thermofisher), 0.1 % Pluronic F68 (Gibco), 0.7 mg/mL Dextran Texas-Red 70,000 MW (Thermofisher), Phire Hot Start II DNA polymerase (Thermofisher) and the corresponding buffer at recommended concentrations was dispersed into 2.5 pL droplets carried by a Novec7500 fluorinated oil (3M) supplemented with 3% of fluorosurfactant as described before (44). The emulsion was collected and thermocycled as above.

ii. In vitro *gene expression*. Upon thermal-cycling, amplified DNA-containing droplets were reinjected into a droplet fusion device where they were synchronized and fused with larger 17 pL on-chip produced droplets (generated as described in (45) containing an *in vitro* expression mixture made of 3 mM of the 20 aminoacids, 1 U/µL RNasin® (Promega), 500 µM of the four NTP, 3 mM $MgCl_2$, 80 mM KCl, 30 µL/mL Dextran Texas-Red 70,000 MW (Thermofisher), 50 µg/mL of T7 RNA polymerase purified in the lab and half of a volume of Rabbit Reticulocyte Lysate prepared as previously described (48). Pairwise droplets were fused, the emulsion was collected as described before (45) and incubated for 3 hours at 30 °C.

iii. Droplet analysis and sort. Upon incubation, droplets were reinjected into a sorting device where they were spaced by a surfactant-free oil stream and their fluorescence was analyzed just before reaching the sorting junction (49). Droplets orange (Texas-red) fluorescence allowed discriminating *in vitro* expression droplets fused to a single PCR droplet from those unfused or fused with more than one PCR droplet as described in (44). Moreover, using the green fluorescence (GFP fluorescence) of these single-fused droplets allowed us to identify and sort those droplets displaying significant concentration of GFP, therefore containing variants able to support efficient translation initiation. The green fluorescence gates used for

each experiment are summarized on Figure S2d and S7a. Upon sorting, the recovered droplets were collected in a tube and broken by adding 50 µL of 1H,1H,2H,2H-perfluoro-1-octanol (Sigma-Aldrich) and 200 µL of 200 µg/mL yeast total RNA solution (Ambion). The selected genes were finally recovered by PCR-amplifying the DNA contained in a 2 µL aliquot of droplet lysate solution and introducing it in 100 µL of PCR reaction mixture containing 0.2 µM of FwdIRES-GFP (5'GTCGTCTAATCCAGAGACCCCGGATCGG3') and RevGFP (5' GAAGCGGCCGCTCTAGATTAATTTAAATC3') primers, 0.2 mM of each dNTP (Thermofisher), 0.04 U/µL of Phusion DNA polymerase (Thermofisher) and the corresponding buffer at the recommended concentration. The mixture was then subjected to an initial denaturation step of 2 min at 95°C followed by 25 cycles of: 30 sec at 95°C, 30 sec at 55°C, 1 min at 72°C, and terminated by a final extension of 10 min at 72°C. The PCR product was then purified on a 1% agarose TBE gel, the band containing the product of interest was excised, the DNA recovered using a "Wizard® SV Gel and PCR Clean-Up System" kit (Promega) and quantified with a Nanodrop (Thermo Scientific). The purified DNA was then either used to start a new round of screening or indexed and sequenced (see below).

The procedure described above was performed in two independent biological replicates using different batches of Rabbit reticulocytes extract. At each round, an average of 1.5 million of droplets were screened corresponding to a minimum of ~ 37.5 times coverage (considering the 10% occupancy of PCR droplets).

Sequence analysis

Libraries indexing and sequencing. A 2 µL aliquot of droplet lysate was introduced in 100 µL of PCR reaction mixture containing 0.2 µM of Label-CrPV-Fwd (5'TCGTCGGCAGCGTCAGATGTGTATAAGAGACAGGGCAAAAATGTGATCTTGC TTGTAAAT 3') and Label-CrPV-Rev (5' GTCTCGTGGGCTCGGAGATGTGTATAAGAGACAGGGGACAACTCCAGTGAAAA GTTCTTC3') primers, 0.2 mM of each dNTP (Thermofisher), 0.04 U/µL of Phusion DNA polymerase (Thermofisher) and the corresponding buffer at the recommended concentration. The mixture was then subjected to an initial denaturation step of 2 min at 95°C followed by 25 cycles of: 30 sec at 95°C, 30 sec at 55°C, 1 min at 72°C, and terminated by a final extension of 10 min at 72°C. PCR products were purified using

a “Wizard® SV Gel and PCR Clean-Up System” kit (Promega). The PCR product was then diluted down to 0.5 ng/µL into 25 µL of a PCR mixture containing 2.5 µL of each Nextera Index primer (Illumina), 0.2 mM of each dNTP (Thermofisher), 0.04 U/µL of Phusion DNA polymerase (Thermofisher) and the corresponding buffer at the recommended concentration. The mixture was subjected to an initial denaturation step of 3 min at 95°C followed by 20 cycles of: 30 sec at 95°C, 30 sec at 55°C, 30 sec at 72°C and the run was concluded by 5 min of final extension at 72°C. PCR products were then purified on a 1% agarose gel as above. Indexed DNA libraries were then quantified as recommended by Illumina, loaded and analyzed on a MiSeq intrument using a MiSeq Reagent kit V2 300 cycles cartridge and a pair-end protocol.

Sequencing data analysis. Fastq data files were analyzed using a custom Python-written pipeline. Briefly, high quality reads (Q-score > 30) were recovered and only those sequences free of mutation outside the randomized region (i.e. codon/anticodon mimicking region) were conserved for the rest of the analysis. Next, we filtered out the experimental noise that corresponded mainly to sequences displaying mutations in the codon/anticodon region as a result of PCR and/or sequencing errors. These sequences were expected to have a significantly lower occurrence than the error-free DNA (a droplet was expected to contain ~ $2.4\ 10^5$ identical copies of the DNA). Therefore, monitoring the occurrence of the different sequences made possible identifying those underrepresented (Figure S2c). Indeed, whereas in the case of evenly represented sequences (e.g. starting library, Figure S2a and b) their occurrences linearly accumulate throughout the sequence population, the presence of a significantly underrepresented sub-population of sequences leads to a biphasic line whom the breakpoint can be used as a signal/noise threshold (Figure S2b). Using this approach, only sequences with an occurrence frequency over the threshold (respectively set to $1.9\ 10^{-3}$ and $2.4\ 10^{-3}$ for replicates 1 and 2 of relaxed selection and set to $3.4\ 10^{-3}$ and $1.6\ 10^{-3}$ respectively for replicates 1 and 2 of stringent selection) were considered has “real” signal (Figure S2c). Furthermore, only sequences reliably found in both replicates were conserved for the establishment of codon/anticodon matrices (Figure S2e and S7a). This led to 97 sequences in the relaxed selection conditions and 55 sequences in the stringent selection conditions. Finally, in the stringent selection conditions, only the 52 sequences shared with those reliably identified in the relaxed selection conditions

were finally considered. The generally larger number of sequences found in replicate 2 correlates well with the apparently less resolutive sort (Figure S2b and c).

tRNA transcript synthesis

tRNAs were *in vitro* transcribed by T7 RNA polymerase from templates generated by primer extension of overlapping DNA oligonucleotides (IDT) and purified on 10% denaturing PAGE. Transcripts were extracted by soaking gel slices two hours at 37 °C in 50 mM KOAc and 200 mM KCl, pH 7, precipitated, and resuspended in H_2O (50).

In vitro translation with rabbit reticulocyte lysates

Translation reactions were performed in self-made RRL extracts as previously described (51). Reactions were incubated at 30 °C for 60 min and included 100 and 200 nM of each reporter mRNA transcript and 10.8 µCi [^{35}S]Met. Aliquots of translation reactions were analyzed by 15% SDS-PAGE and Luciferase assays.

tRNA transfection in HeLa cells and metabolic assay

Adherent HeLa cells were maintained at 37 °C, 5% CO2, in Dulbecco's modified Eagle's medium supplemented with fetal calf serum and antibiotics. Transfections were performed in 96-well plates at 90% confluency with 1.25 pmol (~30ng) or 2.5 pmol (~60ng) of control or impossible tRNAs using Lipofectamine 2000 (Invitrogen) according to manufacturer's instructions (52). Each transfection condition was independently replicated nine times.

Cell proliferation assays were performed 24 hours after transfection by addition of 10 µl (1/10 of the culture volume) of WST-1 (G-biosciences). The formazan dye (yellow) produced by metabolically active cells was quantified using a multi-well spectrophotometer at 450 nm, 30 min after WST-1 addition (53). Unpaired t-tests (GraphPad software package) were performed to evaluate the statistical relevance of the differences in metabolic activities between control and impossible tRNAs.

Data availability

The datasets generated during and/or analysed during the current study are available from the corresponding author on reasonable request.

RESULTS AND DISCUSSION

Ultrahigh-throughput screening of the complete anticodon/codon library

In order to profile exhaustively the different anticodon/codon pairs and identify those accepted and translocated by the ribosome, we designed a droplet-based microfluidic screening pipeline allowing the quantitative measurement of the expression of a Green Fluorescent Protein-coding (GFP) reporter gene. We first prepared a construct in which the IGR IRES from CrPV was placed upstream the GFP coding sequence (Figure 1 and S1). The internal anticodon and codon mimicking sequences embedded in PKI pseudoknot recruit the ribosome and lead to GFP synthesis all the better the anticodon/codon pair is efficiently accepted by the ribosome, which makes possible to directly correlate anticodon/codon acceptancy with a fluorescent signal. Using this construct as a framework, we generated a library containing the 4096 (64 x 64) possible anticodon/codon combinations by randomizing both sequences (Figure 1 and S1). The library was then screened for variant able to support efficient translation (so anticodon/codon pairs readily accepted by the ribosome) using a droplet-based microfluidic workflow (Figure S2a) similar to that previously used to analyze protein (54) and RNA gene libraries (44–47). Briefly, each DNA molecule of the library was individualized with an amplification mixture into picoliter-sized water-in-oil droplets serving as independent vessels. Upon PCR amplification, each droplet was fused one-to-one with a larger droplet containing an *in vitro* coupled transcription and translation mixture allowing genes to be transcribed and resulting mRNA to be translated (55), provided the anticodon/codon pair displayed by PKI is properly accommodated and used by the ribosome. Therefore, constructs in which an IRES-displayed anticodon/codon pair was accepted and validated by the ribosome were expected to support GFP synthesis, turning the corresponding droplets fluorescent and allowing for sorting them (49). Two replicates were performed (Figure S2d) during which our capacity to generate and manipulate millions of such droplets in a single experiment, allowed us to screen the 4096 combinations contained in the starting library with a more than 30-time coverage. Next generation sequencing was then used to assess the completeness of the starting library (Figure S2b and c) and then to identify functional codon/anticodon pairs that were selected (Figure S2e).

Selected cognate codon/anticodon combinations with Watson-Crick base pairs

Throughout this publication, we use the sign "/" to indicate both orientations of base pairs (e.g. A/U for A-U or U-A) and the sign 'o' for standard wobble base between G and U (e.g. GoU for G-U). We found that only 97 combinations are efficiently accepted and translocated by the ribosome (Figure 2). Surprisingly, less than half of the combinations, 38 out of 97, are among the expected complementary Watson-Crick (W-C) pairs between anticodon and cognate codon (black squares on the diagonal of the matrix in Figure 2 and Figure S3). Gaps in the diagonal correspond to the remaining 26 possible W-C combinations that were not selected (Figure 3 and Figure S4). Among these combinations, a significant bias against A/U-content was observed and the higher the A/U content, the less the sequence was recovered (Figure 3a,b and Figure S4). Indeed, only 1 instance out of 8 A/U-free sequence pairs was missing, whereas 6 out of 12 (50 %), 13 out of 24 (54 %) and 6 out of 8 (75%) sequences were missing for sequence pairs containing respectively 1, 2 and 3 A/U base pairs. In 19 out of 26 instances, the missing combinations have a pyrimidine (Y) at the first anticodon position (numbered 34) and thus a purine (R) at position 3 of the codon (Figure S4). These missing combinations include the AUG start codon and the three STOP codons. The only missing W-C combination without an A/U pair is the combination between anticodon CCC and codon GGG (corresponding to Gly)(Figure S4).

The distribution of the missing Watson-Crick combinations absent from the selection is plotted on the wheel representation of the genetic code (56) in Figure 3c. At the north of the wheel are shown the "strong" or G/C-rich codon-anticodon triplets, at the south the "weak" or A/U-rich codon-anticodon triplets and in the middle the "intermediate" ones as measured by the energy (57) of the helical triplet. The A/U-rich missing combinations confirm the contribution of nucleotide modifications in such codon/anticodon triplets to productive decoding in natural systems (58, 59). In five of the codon boxes, all codons are selected (corresponding to the two 4-codon boxes Pro and Arg, and the three 2-codon boxes His, Gln, and Ser). In the selected combinations, three codons were not represented, corresponding to Glu (GAR), Lys (AAR) and Met (AUG). This is also true for the 2-codon boxes corresponding to amino acids Leu (UUR) and Arg (AGR) (see Figure 3c and Figures S5). Please note that we use the corresponding amino acid for commodity but, in the present experimental system, no amino acid is inserted.

Selected near-cognate codon/anticodon combinations

Besides W-C combinations, we also selected a significant number of combinations (59/97) with one or two mismatches at the three positions of the codon (Figure 2 and Figure S5a). Overall, eight types of mismatches are accepted by the ribosome in the present experimental set-up (G/U, G/A, C/A, C/U, A/A, U/U, C/C and G/G). Most mismatches occur at the third position of the codon (Figure S5b-c). Among the observed mismatches, the most frequent ones are G/U, G/A, C/A and C/U (Figure S5c). Although mismatches are generally found in both orientations (Figure S6a), there are two exceptions. First G/U mismatches observed at the third codon position are exclusively of the G34oU3 type and never of the U34oG3 type. Secondly, C/A mismatches at the second position of the codon are found only as C2/A35. Whereas G/U and C/A mismatches are found in all three positions of the triplets, G/A, C/U, A/A, C/C and G/G mismatches are only found in the third position (Figure S5a and c). Overall, the most frequent mismatch is the G/U base pair, which was found 26 times in the 59 combinations. Likewise, *in vivo* the mis-incorporation frequency determined by mass spectrometry is approximately 10^{-3}-10^{-5}, also confirming that G/U are the most frequent mismatches, responsible for 40% of mis-incorporated amino acids (17, 60).

The distribution of mismatches at the first two positions leads to three interesting observations: (1) 7 out of 10 mismatches in the first position are C/A mismatches in both orientations; (2) 8 out of 12 mismatches in the second position are G/U mismatches, 6 are between U2 and G35 and 2 between G2 and U35; (3) only 2 C/A or U/U mismatches are in the second position (see Figures S5c and S6a). Structural data have shown the presence of G/U pairs at both the first and second positions with a “Watson-Crick like” geometry rather than a “wobble” geometry (61). The present data provide further evidence that G/U base pairs can be accommodated not only at the A site of the ribosome decoding centre but can also be efficiently translocated from the A to the P site to proceed with elongation. This is further corroborated by other structural observations showing atypical Watson-Crick-like G/U base pair geometry in the P site of the tRNA (14). Interestingly, C/A mismatches at position 2 are exclusively observed in the C2-A35 orientation (Figure S6a). Finally, G/A mismatches in both orientations are only observed in position 3 of the codon. G/A is a mismatch involving two large bases that can coexist only in position 3 but

not in position 1 and 2 due to tighter steric constraints (62). The same reasoning likely applies to G/G and A/A mismatches that are also observed only in position 3 of the codon (Figure S5).

Interestingly, only 17 near-cognate events would lead to amino acid change (in normal ribosomal translation) and all those involve a G34-containing anticodon (see Fig. S8 and below).

To further corroborate the selection matrix, we chose several representative selected combinations, namely purely W-C combinations, combinations containing mismatches with a few combinations that were not selected taken as negative controls. We inserted them in a reporter mRNA containing the IGR upstream of the Renilla luciferase coding region in order to measure the corresponding translation efficiency. Using this experimental set-up, we determined that the present microfluidic pipeline allowed us to select combinations that promote translation efficiency above 20% compared to the Wt IGR (Figure S6b). Likewise, we confirmed the preferential orientation of G34/U3 mismatch at position 3 of the codon as deduced from the selection results (Figure S6c).

The types of selected combinations indicate that the IRES-based microfluidic pipeline recapitulates faithfully cellular decoding rules

a) A/U rich combinations require modification in the anticodon

In cells, tRNAs contain critical nucleotide modifications in the ASL. Although every anticodon nucleotide can be modified, positions 32, 34, 37, and 38 (Figure S1) play critical roles in translation fidelity (63, 64). In the present *in vitro* transcribed PKI and its associated IGR-GFP reporter, these modified nucleotides are absent. The observation that nearly all of the missing W-C combinations contain between one and three A/U base pairs strongly suggests that A/U base pairs are weak interactions not stable enough on the ribosome to allow efficient translocation without modifications in the tRNA ASL (63). Especially, the lack of modifications also correlates with the absence in the selected pools of combinations with A or U at the 1st and 3rd positions of the codon. Both require modifications at either position 37 (63) or at position 34

(16, 65) of the anticodon, respectively (see below) (Figure S1). There is particularly a poor representation of combinations with a U or a C at the first position 34 of the anticodon (19 out of 26 cases), indeed U34 and C34 are nucleotides that are frequently modified in tRNAs (16, 65) (Figure 3b).
As expected, the absence of modified nucleotides in the PKI of the reporter IGR-GFP does not allow the selection of the A/U-rich codon-anticodon combinations since there are not stable enough on the ribosome and cannot promote GFP translation. Thus, the gaps in the W-C diagonal mainly correspond to codons that require post-transcriptional modifications in the tRNA ASL to be efficiently decoded by the eukaryotic ribosome.

b) Position 3 of the codon is the most permissive

Among the three positions of the codon, it is expected that position 3 of the codon is the most permissive one (66). As expected, most of the mismatches are observed on position 3 of the codon (Figure S5b-c). This is consistent with fundamental decoding rules in both prokaryotic and eukaryotic ribosomes (66).

c) Most of the G34/U3 wobble combinations are efficiently selected

Remarkably, 12 of the 16 possible combinations with a G34oU3 pair were selected; the four missing ones contain A/U base pairs at positions 1 and/or 2 in addition to the G34oU3, which suggests that the binding affinity of the corresponding complexes is too low to support translational activity in the modification-free PKI. Standard wobble base pairs between G and U are widely used in cells for decoding synonymous codons; the observation that the present system selected almost all of them confirms that PKI accurately mimics the structure and the function of a genuine codon/anticodon mini helix on the ribosome. Additional evidence comes from the asymmetry observed in the G/U pairs at the third position where only G34oU3 and not the inverted U34oG3 base pair was observed. This observation is in agreement with crystallographic data showing the expected G34oU3 wobble pair while the U34oG3 pair was observed only in presence of U34 modification and then only in a tautomeric Watson-Crick-like geometry (67) or in a novel type of pair in which the U instead of moving in the major groove as in standard wobble pair moves in the minor

groove (68). These alternative geometries are imposed by the ribosome decoding centre grip together with the presence of modified nucleotides shaping the ASL and the codon/anticodon helix (16, 56). Using a Renilla luciferase reporter assay, we confirmed that such a preferential orientation is also observed in the context of the IGR PKI, which again confirms that PKI is a biologically relevant mimic of the codon-anticodon helix (Figure S6c).

d) The most frequently accepted mismatches are G/U, G/A and C/A.

In order to assess the efficiency of the selected codon-anticodon combinations to promote translation, we re-screened the enriched libraries from both replicates and performed another screen with a higher sorting cut-off (only the 50% most fluorescent droplets displaying a signal above the background were recovered) and (this new selection was called 'stringent selection') (Figure S7a/b). Under these 'stringent' conditions, only 52 combinations are present in both replicates ((Figure S7b). However, the distribution of mismatches is similar to the first selection, again most of the mismatches are observed on position 3 of the codon. The combinations containing the G34oU3 wobble mismatch are still largely represented (10/16 possible combinations). Moreover, the combinations contain only three types of mismatches G/U, G/A and C/A indicating that they are better accepted by the ribosome. Interestingly, triplets involving G/U, G/A and C/U mismatches are responsible for the most prevalent amino acid substitutions observed *in vivo* (60). In contrast, A/A, U/U, C/C and G/G are not present in the 'stringent' selection, suggesting that they are less efficiently tolerated by the ribosome, which is in agreement with *in vivo* observations.
We realize that the PKI-based reporter system does not fully mimic a tRNA anticodon-codon duplex. First, unlike tRNA molecules, the IRES is delivered to the ribosome in the absence of elongation factors, therefore the system eliminates initial selection of cognate tRNA molecules and competition between tRNAs and factors. Secondly, the IRES forms extensive contacts with the ribosome compared to tRNAs and in the IRES structure, the 'anticodon-like' triplet is covalently linked to the 'codon-like' triplet. Such factors could affect tRNA selection and proofreading in the A site. Nevertheless, the results of the selections strongly indicate that the PKI-based microfluidic-assisted selection using an IGR-GFP reporter system does recapitulate faithfully most fundamental aspects of both bacterial and eukaryotic decoding.

Altogether, the present data suggest that eukaryotic ribosomes (rabbit) follow the same basic geometrical rules as the bacterial decoding centre (68) and that decoding centres across the different domains of life likely share a similar if not identical structural grip.

More than half of the combinations contain G34 in the anticodon

Unexpectedly, the majority of the selected combinations (51/97, 52.6%) contained G34 in the anticodon (Figure 2). These comprise 15 W-C combinations G34-C3 (15 of the 16 possible), 12 wobble combinations G34-U3 (12 of the 16 possible) suggesting that combinations with a G34 are well accepted by the ribosome. Surprisingly, G34 is also present in 24 combinations containing mismatches (Figure 2), suggesting the sole presence of G34 allows mismatches at the three positions of the codon. In terms of decoding, the consequence of such mismatches would be detrimental for translation fidelity. Indeed, many of these combinations would promote miscoding issues because they enable base pairing of tRNA anticodons with near-cognate codons (Figure S8). The resulting potential miscoding errors are almost exclusively observed in the decoding of the 4-codon boxes (equivalent to Leu (CUN), Ala, Val, Thr, Ser (UCN), Pro, Arg (CGN) and Gly). The high occurrence of mismatches in combinations with G34 prompted us to examine the distribution of G34 in tRNA genes decoding the 4-codon boxes from several eukaryotic species. As previously shown (65), G34-containing tRNAs are very rarely found in eukaryotic tRNAs that decode 4-codon boxes (Figure 4a and Figure S9). Indeed G34-containing tRNAs are virtually absent from all eukaryotic genomes in the tRNAs decoding 4-codon boxes; A34 tRNAs (normally modified into I34, see for example (69)) are used instead. Gly is the only exception for which, in all three kingdoms, a G34-containing tRNA decodes the C3- and U3-ending codons (and A34 is never observed (65)). In contrast to bacterial tRNAs for Gly, the eukaryotic $tRNA^{Gly}$ do not exhibit the potential for 32-38 WC pair (mainly C/C or C/A in all eukaryotes tested on the GtRNAdb database (70)). Explanations have been suggested for the presence of eukaryotic G34-containing $tRNA^{Gly}$: structural incompatibility of A34 in the anticodon loop (71) or frame maintenance (72). We note also the conserved presence of GU pairs in the alignments of anticodon stem of eukaryotic $tRNA^{Gly}$ (70).

tRNAs with G34 are toxic miscoders in eukaryotes

The microfluidic-assisted screenings hinted that a G34 in the anticodon of tRNA decoding 4-box codons is potentially detrimental for translation fidelity in eukaryotes due to an increased miscoding capability. Since these tRNAs are virtually absent from eukaryotic genomes, we named such tRNAs “impossible tRNAs” or itRNAs. In order to investigate the origin of the counter-selection against itRNAs during eukaryotic evolution, we assembled those species artificially. For that purpose, we synthesized control/wild type human $tRNA^{Ala,Pro,Thr,Ser,Leu}$ containing A34 and their corresponding itRNA counterparts in which only the nucleotide A34 , was substituted by G34. We then transfected them into human HeLa cells and assessed cellular fitness through a standard WST-1 metabolic assay (Figure 4b). Strictly speaking WST-1 assays directly measure the metabolization of formazan by mitochondria. Mitochondrial fitness is a widely accepted proxy for the overall cellular fitness. Although the rate of protein synthesis very often correlates with cellular health, WST-1 assays should not be used to directly assess the dynamic of translation. We would like to emphasize that we did not employ WST-1 assay to draw conclusions on the effects of our tRNA constructs on translation. As anticipated from the microfluidic screenings, when G34 is present, the cell general metabolism is significantly affected indicating that $itRNA^{Ala,Pro,Thr,Leu}$ are indeed toxic to a certain degree, $itRNA^{Ser}$ with a G34 being the only non-toxic itRNA. To demonstrate that the toxicity is actually due to miscoding induced by itRNAs, we used human $tRNA^{Ala}$ as a scaffold to test the impact of G34-containing anticodons. We assembled different chimeras $tRNA^{Ala}$ displaying ambiguous G34-anticodons (Figure 4c). The alanine system is best suited to anticodon manipulation because human alanyl-tRNA synthetase (AlaRS) discriminates $tRNA^{Ala}$ solely by recognizing the unique feature G3-U70 in the acceptor stem of the tRNA (73, 74). Therefore, it is possible to change the whole anticodon of $tRNA^{Ala}$ without affecting its ability to be alanylated by AlaRS. We generated human $tRNA^{Ala}$ transcripts containing the following G34-anticodons (G34GG, G34GC, G34GA, G34AG) and AGC the alanine anticodon as a negative control. Miscoding capacity was measured with a reporter C-terminally HA-tagged Renilla luciferase gene in which we introduced silent mutations to enrich the luciferase coding sequence in codons prone to be potentially misdecoded by itRNAs according to the combinations that were identified from the microfluidic screenings

(Figure S8). Reporter mRNAs were then translated *in vitro* using rabbit reticulocyte lysates and the different $tRNA^{Ala}$ chimeras. None of the $tRNA^{Ala}$ constructs affected the overall translation yield of Renilla reporter protein in a significant way (Figure 4d). However, the luciferase activity was significantly affected in the presence of hybrid tRNA transcripts containing GGG, GGA and GAG anticodons suggesting that these tRNAs promote alanine insertion at unexpected positions in the Renilla luciferase coding sequence thereby affecting the luciferase activity (Figure 4e). To demonstrate the miscoding capability of these chimeric $tRNA^{Ala}$ transcripts, we purified the produced Renilla luciferase protein using a C-terminal HA-tag. Mass spectrometry analysis of *in vitro* synthesized and purified luciferase revealed the presence of peptides containing alanine residues at mutated codons. These residues were inserted by the chimeric tRNAs at non-alanine codons indicating that the transcripts are efficiently aminoacylated by AlaRS and functional in the ribosome (Figure S10a). We also found another peptide containing an alanine residue that was inserted by $tRNA^{Ala}_{GGA}$ at a CCC codon. Therefore, we show that this hybrid $tRNA^{Ala}_{GGA}$ promotes miscoding of a CCC codons, demonstrating without ambiguity that G at position 34 allows the decoding of non-cognate CCC codons displaying a C/A mismatch at codon position 1 (C1/A36) (Figure S10b). Remarkably, this unexpected $_{1}CCC_{3}/_{34}GGA_{36}$ combination is one of those identified in the microfluidic-based screening (marked by an asterisk in Figure S8). Altogether, these experiments confirm that in a eukaryotic system the sole presence of G34 in tRNAs decoding 4-codon boxes induces miscoding induced by the formation of mismatches at position 1 and 2 of the codon.

Nucleotides 32 and 38 correlate with R34 in 4-codon boxes

Very specific covariations at nucleotides 32 and 38 (as well as 31 and 39) were shown to participate in the anticodon loop conformation (58, 75, 76) and in the modulation of the codon/anticodon interactions (42). Early experiments showed the role of nucleotide 32 for discriminating the Gly codons (77, 78). Later, experiments on *E.coli* $tRNA^{Ala}$ (G34CC) revealed that the nucleotides A32 and U38 in this tRNA were critical for accurate decoding (79, 80). Indeed, when 32-38 could not form a potential Watson-Crick pair (e.g. A32 and C38), the mutated $tRNA^{Ala}$ promoted miscoding and lethal toxicity in bacteria. This prompted us to examine the distribution of nucleotides

32 and 38 in *Homo sapiens*. In contrast to prokaryotes, nucleotides 32 and 38 are not complementary in any 4-codon box tRNA (Figure 5). By analogy to the prokaryotic tRNAs, we then speculated that the toxicity induced by G34 in itRNAs was actually anticorrelated with the potential for nucleotides 32 and 38 to form a standard Watson-Crick pair in these tRNAs. In order to demonstrate this, we introduced in the toxic $tRNA^{Ala,Pro,Thr,Leu}$-G34, a point mutation that enables Watson-Crick base pairing between nucleotides 32 and 38 (Figure 5). As predicted, $tRNA^{Ala,Pro,Leu}$, for which the itRNA counterparts are the most toxic, are not toxic anymore when 32-38 can form a Watson-Crick base pair. Unexpectedly, this is not the case for $tRNA^{Thr}$-G34, which is more toxic with a 32-38 base pair. In contrast to the three others, the wt $tRNA^{Thr}$ contains a m^3C32 that could be critical for other enzymatic reactions such as aminoacylation or tRNA modification. m^3C32 is positively charged and the effects of the introduction of such a modification are unknown. Overall, these results confirm that G34 is toxic in such tRNAs only when nucleotides 32-38 cannot form a standard Watson-Crick pair.

Nucleotides 32 and 38 are respectively at the beginning and end of the anticodon loop just following the anticodon stem. The presence of complementary bases at those two positions can induce the formation of an additional base pair in the anticodon stem. This introduces an additional rotation to the stem and re-orients the anticodon triplet in an unfavourable position for base pairing with the codon triplet. In other words, the conformation of the anticodon is no longer properly pre-organized for productive base pairing with the codon (76, 78–80). Such a terminal 32-38 base pair is naturally dynamic and only some fraction of the tRNA population will at any moment contain the base pair. By mass action, this automatically leads to a reduction in the free energy of tRNA-mRNA binding (42). This mechanism applies particularly to tRNAs forming G/C-rich anticodon/codon triplets where U32/A38 occurs instead of the more common C32/A38. In the early experiments mentioned above (77, 78), replacing U32 by C32 led to an undiscriminating tRNA. The replacement of G34 by A34 (modified in I34) leads to base pairings with less energy content. Thus, strong G34-containing tRNAs would favour nucleotide combinations at 32 and 38 that are able to form a Watson-Crick pair, while weak A34(I34)-containing tRNAs will not need this additional tRNA constraints.

In conclusion, the combined use of a microfluidic-based analysis pipeline and of cell-free translation extracts faithfully recapitulates the main structural trends of molecular recognition in eukaryotic translation. The data show that, in the absence of competitor tRNAs, release factors and protein sequence effects, productive translation relies entirely on the stability of the codon/anticodon triplet. In addition, in the absence of tRNA modifications in the anticodon loop, tRNA binding to the ribosomal decoding centre is either unproductive or leads to extensive miscoding, especially with G34-containing tRNAs. Finally, the nature of the base at R34-containing tRNAs correlates with nucleotide conservations at positions 32 and 38 for smooth decoding: G34-tRNAs favor combinations of 32 and 38 that have the potential to form a Watson-Crick pair while A34-tRNAs do not. Bacteria evolved to maintain G34 and the constraint on 32 and 38, while eukaryotes selected A34(I34) instead.

Acknowledgments

This work was funded by 'Agence Nationale pour la Recherche' (Ribofluidix, ANR-17-CE12-0025-01/02 and RFS, ANR-15-CE11-0021-01), by University of Strasbourg (PEPS 2015- IDEX) and by the 'Centre National de la Recherche Scientifique', This work has also been published under the framework of the LabEx: ANR-10-LABX-0036_NETRNA and benefits from a funding from the state managed by the French National Research Agency as part of the Investments for the future program. We are grateful to Friedrich Preusser, Fatima Alghoul and Lauriane Gross for technical assistance and we also warmly thank Sandrine Koechler and Abdelmalek Alioua from the IBMP Gene Expression Analysis facility for technical assistance with high-throughput sequencing. The facility is supported and funded as part of the LabEx NetRNA and MitoCross. The mass spectrometry instrumentation was granted from Université de Strasbourg (IdEx 2015 Equipement mi-lourd).

References

1. Drummond,D.A. and Wilke,C.O. (2008) Mistranslation-Induced Protein Misfolding as a Dominant Constraint on Coding-Sequence Evolution. *Cell*, **134**, 341–352.
2. Ruan,B., Palioura,S., Sabina,J., Marvin-Guy,L., Kochhar,S., LaRossa,R.A. and Soll,D. (2008) Quality control despite mistranslation caused by an ambiguous genetic code. *Proc. Natl. Acad. Sci.*, **105**, 16502–16507.
3. Kohanski,M.A., Dwyer,D.J., Wierzbowski,J., Cottarel,G. and Collins,J.J. (2008) Mistranslation of Membrane Proteins and Two-Component System Activation Trigger Antibiotic-Mediated Cell Death. *Cell*, **135**, 679–690.
4. Mohler,K., Mann,R. and Ibba,M. (2017) Isoacceptor specific characterization of tRNA aminoacylation and misacylation in vivo. *Methods*, **113**, 127–131.
5. Francklyn,C.S. (2008) DNA polymerases and aminoacyl-tRNA synthetases: Shared mechanisms for ensuring the fidelity of gene expression. *Biochemistry*, **47**, 11695–11703.
6. Soll,D. (1990) The accuracy of aminoacylation--ensuring the fidelity of the genetic code. *Experientia*, **46**, 1089–1096.
7. Ribas de Pouplana,L., Santos,M.A.S., Zhu,J.H., Farabaugh,P.J. and Javid,B. (2014) Protein mistranslation: Friend or foe? *Trends Biochem. Sci.*, **39**, 355–362.
8. Jørgensen,F. and Kurland,C.G. (1990) Processivity errors of gene expression in Escherichia coli. *J. Mol. Biol.*, **215**, 511–21.
9. Wohlgemuth,I., Pohl,C., Mittelstaet,J., Konevega,A.L. and Rodnina,M. V (2011) Evolutionary optimization of speed and accuracy of decoding on the ribosome. *Philos. Trans. R. Soc. B Biol. Sci.*, **366**, 2979–2986.
10. Manickam,N., Nag,N., Abbasi,A., Patel,K. and Farabaugh,P.J. (2014) Studies of translational misreading in vivo show that the ribosome very efficiently discriminates against most potential errors. *RNA*, **20**, 9–15.
11. Parker,J. (1989) Errors and alternatives in reading the universal genetic code. *Microbiol. Rev.*, **53**, 273–98.
12. Kramer,E.B. and Farabaugh,P.J. (2007) The frequency of translational misreading errors in E. coli is largely determined by tRNA competition. *RNA-a Publ. RNA Soc.*, **13**, 87–96.
13. Kramer,E.B., Vallabhaneni,H., Mayer,L.M. and Farabaugh,P.J. (2010) A comprehensive analysis of translational missense errors in the yeast Saccharomyces cerevisiae. *Rna*, **16**, 1797–1808.
14. Demeshkina,N., Jenner,L., Westhof,E., Yusupov,M. and Yusupova,G. (2012) A new understanding of the decoding principle on the ribosome. *Nature*, **484**, 256–259.
15. Rozov,A., Demeshkina,N., Westhof,E., Yusupov,M. and Yusupova,G. (2015) Structural insights into the translational infidelity mechanism. *Nat. Commun.*, **6**, 7251.
16. Rozov,A., Demeshkina,N., Khusainov,I., Westhof,E., Yusupov,M. and Yusupova,G. (2016) Novel base-pairing interactions at the tRNA wobble position crucial for accurate reading of the genetic code. *Nat. Commun.*, **7**, 10457.
17. Rozov,A., Wolff,P., Grosjean,H., Yusupov,M., Yusupova,G. and Westhof,E. (2018) Tautomeric G•U pairs within the molecular ribosomal grip and fidelity of decoding in bacteria. *Nucleic Acids Res.*, **46**, 7425–7435.
18. Rodnina,M. V and Wintermeyer,W. (2011) The ribosome as a molecular machine: the mechanism of tRNA-mRNA movement in translocation. *Biochem. Soc. Trans.*, **39**, 658–62.
19. Voorhees,R.M. and Ramakrishnan,V. (2013) Structural basis of the translational elongation cycle. TL - 82. *Annu. Rev. Biochem.*, **82**, 203–236.

20. Demeshkina,N., Jenner,L., Yusupova,G. and Yusupov,M. (2010) Interactions of the ribosome with mRNA and tRNA. *Curr. Opin. Struct. Biol.*, **20**, 325–332.
21. Wilson,J.E., Powell,M.J., Hoover,S.E. and Sarnow,P. (2000) Naturally occurring dicistronic cricket paralysis virus RNA is regulated by two internal ribosome entry sites. *Mol. Cell. Biol.*, **20**, 4990–4999.
22. Sasaki,J. and Nakashima,N. (1999) Translation initiation at the CUU codon is mediated by the internal ribosome entry site of an insect picorna-like virus in vitro. *J. Virol.*, **73**, 1219–1226.
23. Pestova,T. V, Lomakin,I.B. and Hellen,C.U.T. (2004) Position of the CrPV IRES on the 40S subunit and factor dependence of IRES/80S ribosome assembly. *EMBO Rep.*, **5**, 906–13.
24. Schuler,M., Connell,S.R., Lescoute,A., Giesebrecht,J., Dabrowski,M., Schroeer,B., Mielke,T., Penczek,P.A., Westhof,E. and Spahn,C.M. (2006) Structure of the ribosome-bound cricket paralysis virus IRES RNA. *Nat. Struct. Mol. Biol.*, **13**, 1092–1096.
25. Pestova,T. V. and Hellen,C.U.T. (2003) Translation elongation after assembly of ribosomes on the Cricket paralysis virus internal ribosomal entry site without initiation factors or initiator tRNA. *Genes Dev.*, **17**, 181–186.
26. Costantino,D. and Kieft,J.S. (2005) A preformed compact ribosome-binding domain in the cricket paralysis-like virus IRES RNAs. *RNA*, **11**, 332–343.
27. Filbin,M.E. and Kieft,J.S. (2009) Toward a structural understanding of IRES RNA function. *Curr. Opin. Struct. Biol.*, **19**, 267–76.
28. Au,H.H., Cornilescu,G., Mouzakis,K.D., Ren,Q., Burke,J.E., Lee,S., Butcher,S.E. and Jan,E. (2015) Global shape mimicry of tRNA within a viral internal ribosome entry site mediates translational reading frame selection. *Proc. Natl. Acad. Sci. U. S. A.*, **112**, E6446-55.
29. Spahn,C.M.T., Jan,E., Mulder,A., Grassucci,R.A., Sarnow,P. and Frank,J. (2004) Cryo-EM visualization of a viral internal ribosome entry site bound to human ribosomes: The IRES functions as an RNA-based translation factor. *Cell*, **118**, 465–475.
30. Fernàndez,I.S., Bai,X.C., Murshudov,G., Scheres,S.H.W. and Ramakrishnan,V. (2014) Initiation of translation by cricket paralysis virus IRES requires its translocation in the ribosome. *Cell*, **157**, 823–831.
31. Costantino,D.A., Pfingsten,J.S., Rambo,R.P. and Kieft,J.S. (2008) tRNA-mRNA mimicry drives translation initiation from a viral IRES. *Nat. Struct. Mol. Biol.*, **15**, 57–64.
32. Koh,C.S., Brilot,A.F., Grigorieff,N. and Korostelev,A.A. (2014) Taura syndrome virus IRES initiates translation by binding its tRNA-mRNA-like structural element in the ribosomal decoding center. *Proc. Natl. Acad. Sci. U. S. A.*, **111**, 9139–44.
33. Murray,J., Savva,C.G., Shin,B.-S., Dever,T.E., Ramakrishnan,V. and Fernández,I.S. (2016) Structural characterization of ribosome recruitment and translocation by type IV IRES. *Elife*, **5**.
34. Hussain,T., Llácer,J.L., Fernández,I.S., Munoz,A., Martin-Marcos,P., Savva,C.G., Lorsch,J.R., Hinnebusch,A.G. and Ramakrishnan,V. (2014) Structural Changes Enable Start Codon Recognition by the Eukaryotic Translation Initiation Complex. *Cell*, **159**, 597–607.
35. Erzberger,J.P., Stengel,F., Pellarin,R., Zhang,S., Schaefer,T., Aylett,C.H.S., Cimermančič,P., Boehringer,D., Sali,A., Aebersold,R., *et al.* (2014) Molecular architecture of the 40S·eIF1·eIF3 translation initiation complex. *Cell*, **158**, 1123–35.
36. Kanamori,Y. and Nakashima,N. (2001) A tertiary structure model of the internal ribosome entry site (IRES) for methionine-independent initiation of translation.

RNA, **7**, 266–274.
37. Jan,E. and Sarnow,P. (2002) Factorless ribosome assembly on the internal ribosome entry site of cricket paralysis virus. *J. Mol. Biol.*, **324**, 889–902.
38. Yamamoto,H., Nakashima,N., Ikeda,Y. and Uchiumi,T. (2007) Binding mode of the first aminoacyl-tRNA in translation initiation mediated by Plautia stali intestine virus internal ribosome entry site. *J. Biol. Chem.*, **282**, 7770–7776.
39. Zhu,J., Korostelev,A., Costantino,D. a, Donohue,J.P., Noller,H.F. and Kieft,J.S. (2011) Crystal structures of complexes containing domains from two viral internal ribosome entry site (IRES) RNAs bound to the 70S ribosome. *Proc. Natl. Acad. Sci. U. S. A.*, **108**, 1839–1844.
40. Petrov,A., Grosely,R., Chen,J., O'Leary,S.E. and Puglisi,J.D. (2016) Multiple Parallel Pathways of Translation Initiation on the CrPV IRES. *Mol. Cell*, **62**, 92–103.
41. Muhs,M., Hilal,T., Mielke,T., Skabkin,M.A., Sanbonmatsu,K.Y., Pestova,T. V. and Spahn,C.M.T. (2015) Cryo-EM of ribosomal 80s complexes with termination factors reveals the translocated cricket paralysis virus IRES. *Mol. Cell*, **57**, 422–433.
42. Pisareva,V.P., Pisarev,A. V and Fernández,I.S. (2018) Dual tRNA mimicry in the cricket paralysis virus IRES uncovers an unexpected similarity with the hepatitis C virus IRES. *Elife*, **7**.
43. Woronoff,G., Ryckelynck,M., Wessel,J., Schicke,O., Griffiths,A.D. and Soumillion,P. (2015) Activity-Fed Translation (AFT) Assay: A New High-Throughput Screening Strategy for Enzymes in Droplets. *Chembiochem*, **16**, 1343–1349.
44. Ryckelynck,M., Baudrey,S., Rick,C., Marin,A., Coldren,F., Westhof,E. and Griffiths,A.D. (2015) Using droplet-based microfluidics to improve the catalytic properties of RNA under multiple-turnover conditions. *RNA*, **21**, 458–469.
45. Autour,A., Westhof,E. and Ryckelynck,M. (2016) ISpinach: A fluorogenic RNA aptamer optimized for in vitro applications. *Nucleic Acids Res.*, **44**, 2491–2500.
46. Autour,A., Jeng,S.C.Y., Cawte,A.D., Abdolahzadeh,A., Galli,A., Panchapakesan,S.S.S., Rueda,D., Ryckelynck,M. and Unrau,P.J. (2018) Fluorogenic RNA Mango aptamers for imaging small non-coding RNAs in mammalian cells. *Nat. Commun.*, **9**, 656.
47. Bouhedda,F., Fam,K.T., Collot,M., Autour,A., Marzi,S., Klymchenko,A. and Ryckelynck,M. (2019) A dimerization-based fluorogenic dye-aptamer module for RNA imaging in live cells. *Nat. Chem. Biol.*, **16**, 69–76.
48. Pelham,H.R.B. and Jackson,R.J. (1976) An Efficient mRNA-Dependent Translation System from Reticulocyte Lysates. *Eur. J. Biochem.*, **67**, 247–256.
49. Baret,J.-C., Miller,O.J., Taly,V., Ryckelynck,M., El-Harrak,A., Frenz,L., Rick,C., Samuels,M.L., Hutchison,J.B., Agresti,J.J., *et al.* (2009) Fluorescence-activated droplet sorting (FADS): efficient microfluidic cell sorting based on enzymatic activity. *Lab Chip*, **9**, 1850.
50. Eriani,G., Karam,J., Jacinto,J., Richard,E.M. and Geslain,R. (2015) MIST, a novel approach to reveal hidden substrate specificity in aminoacyl-tRNA synthetases. *PLoS One*, **10**, e0130042.
51. Martin,F., Barends,S., Jaeger,S., Schaeffer,L., Prongidi-Fix,L. and Eriani,G. (2011) Cap-Assisted Internal Initiation of Translation of Histone H4. *Mol. Cell*, **41**, 197–209.
52. Geslain,R. and Pan,T. (2010) Functional Analysis of Human tRNA Isodecoders. *J. Mol. Biol.*, **396**, 821–831.
53. Geslain,R., Cubells,L., Bori-Sanz,T., Álvarez-Medina,R., Rossell,D., Martí,E. and de Pouplana,L.R. (2010) Chimeric tRNAs as tools to induce proteome damage and identify components of stress responses. *Nucleic Acids Res.*, **38**, e30.
54. Fallah-Araghi,A., Baret,J.-C., Ryckelynck,M. and Griffiths,A.D. (2012) A completely in

vitro ultrahigh-throughput droplet-based microfluidic screening system for protein engineering and directed evolution. *Lab Chip*, **12**, 882.
55. Mazutis,L., Araghi,A.F., Miller,O.J., Baret,J.C., Frenz,L., Janoshazi,A., Taly,V., Miller,B.J., Hutchison,J.B., Link,D., *et al.* (2009) Droplet-based microfluidic systems for high-throughput single DNA molecule isothermal amplification and analysis. *Anal. Chem.*, **81**, 4813–4821.
56. Grosjean,H. and Westhof,E. (2016) An integrated, structure- and energy-based view of the genetic code. *Nucleic Acids Res.*, **44**, 8020–8040.
57. Chen,J.L., Dishler,A.L., Kennedy,S.D., Yildirim,I., Liu,B., Turner,D.H. and Serra,M.J. (2012) Testing the nearest neighbor model for canonical RNA base pairs: Revision of GU parameters. *Biochemistry*, **51**, 3508–3522.
58. Olejniczak,M., Dale,T., Fahlman,R.P. and Uhlenbeck,O.C. (2005) Idiosyncratic tuning of tRNAs to achieve uniform ribosome binding. *Nat. Struct. Mol. Biol.*, **12**, 788–793.
59. Fahlman,R.P., Dale,T. and Uhlenbeck,O.C. (2004) Uniform binding of aminoacylated transfer RNAs to the ribosomal A and P sites. *Mol. Cell*, **16**, 799–805.
60. Zhang,Z., Shah,B. and Bondarenko,P. V (2013) G/U and certain wobble position mismatches as possible main causes of amino acid misincorporations. *Biochemistry*, **52**, 8165–8176.
61. Rozov,A., Westhof,E., Yusupov,M. and Yusupova,G. (2016) The ribosome prohibits the G•U wobble geometry at the first position of the codon-anticodon helix. *Nucleic Acids Res.*, **44**, 6434–41.
62. Murphy,F. V and Ramakrishnan,V. (2004) Structure of a purine-purine wobble base pair in the decoding center of the ribosome. *Nat. Struct. Mol. Biol.*, **11**, 1251–1252.
63. Machnicka,M.A., Milanowska,K., Oglou,O.O., Purta,E., Kurkowska,M., Olchowik,A., Januszewski,W., Kalinowski,S., Dunin-Horkawicz,S., Rother,K.M., *et al.* (2013) MODOMICS: A database of RNA modification pathways - 2013 update. *Nucleic Acids Res.*, **41**.
64. Björk,G.R. and Hagervall,T.G. (2014) Transfer RNA Modification: Presence, Synthesis, and Function. *EcoSal Plus*, **6**.
65. Grosjean,H., de Crécy-Lagard,V. and Marck,C. (2010) Deciphering synonymous codons in the three domains of life: Co-evolution with specific tRNA modification enzymes. *FEBS Lett.*, **584**, 252–264.
66. Crick,F.H.C. (1966) Codon—anticodon pairing: The wobble hypothesis. *J. Mol. Biol.*, **19**, 548–555.
67. Weixlbaumer,A., Murphy,F. V, Dziergowska,A., Malkiewicz,A., Vendeix,F.A.P., Agris,P.F. and Ramakrishnan,V. (2007) Mechanism for expanding the decoding capacity of transfer RNAs by modification of uridines. *Nat. Struct. Mol. Biol.*, **14**, 498–502.
68. Rozov,A., Demeshkina,N., Westhof,E., Yusupov,M. and Yusupova,G. (2016) New Structural Insights into Translational Miscoding. *Trends Biochem. Sci.*, **41**, 798–814.
69. Auxilien,S., Crain,P.F., Trewyn,R.W. and Grosjean,H. (1996) Mechanism, specificity and general properties of the yeast enzyme catalysing the formation of inosine 34 in the anticodon of transfer RNA. *J. Mol. Biol.*, **262**, 437–458.
70. Chan,P.P. and Lowe,T.M. (2016) GtRNAdb 2.0: An expanded database of transfer RNA genes identified in complete and draft genomes. *Nucleic Acids Res.*, 10.1093/nar/gkv1309.
71. Saint-Léger,A., Bello,C., Dans,P.D., Torres,A.G., Novoa,E.M., Camacho,N., Orozco,M., Kondrashov,F.A. and De Pouplana,L.R. (2016) Saturation of recognition elements blocks evolution of new tRNA identities. *Sci. Adv.*, 10.1126/sciadv.1501860.

72. Janvier,A., Despons,L., Schaeffer,L., Tidu,A., Martin,F. and Eriani,G. (2019) A tRNA-mimic strategy to explore the role of G34 of tRNAGly in translation and codon frameshifting. *Int. J. Mol. Sci.*, **20**, 3911.
73. McClain,W.H., Chen,Y.M., Foss,K. and Schneider,J. (1988) Association of transfer RNA acceptor identity with a helical irregularity. *Science*, **242**, 1681–4.
74. Hou,Y.M. and Schimmel,P. (1988) A simple structural feature is a major determinant of the identity of a transfer RNA. *Nature*, **333**, 140–5.
75. Auffinger,P. and Westhof,E. (2001) An extended structural signature for the tRNA anticodon loop. *RNA*, **7**, 334–341.
76. Olejniczak,M. and Uhlenbeck,O.C. (2006) tRNA residues that have coevolved with their anticodon to ensure uniform and accurate codon recognition. *Biochimie*, **88**, 943–950.
77. Lustig,F., Borén,T., Claesson,C., Simonsson,C., Barciszewska,M. and Lagerkvist,U. (1993) The nucleotide in position 32 of the tRNA anticodon loop determines ability of anticodon UCC to discriminate among glycine codons. *Proc. Natl. Acad. Sci. U. S. A.*, **90**, 3343–3347.
78. Claesson,C., Lustig,F., Borén,T., Simonsson,C., Barciszewska,M. and Lagerkvist,U. (1995) Glycine codon discrimination and the nucleotide in position 32 of the anticodon loop. *J. Mol. Biol.*, **247**, 191–196.
79. Murakami,H., Ohta,A. and Suga,H. (2009) Bases in the anticodon loop of tRNAGGCAla prevent misreading. *Nat. Struct. Mol. Biol.*, **16**, 353–358.
80. Ledoux,S., Olejniczak,M. and Uhlenbeck,O.C. (2009) A sequence element that tunes Escherichia coli tRNAGGCAla to ensure accurate decoding. *Nat. Struct. Mol. Biol.*, **16**, 359–364.

Figure legends:

Figure 1: Microfluidic pipeline for high throughput screening of active codon-anticodon pairs.

The Cricket Paralysis Virus IGR IRES was inserted in the 5'UTR of a reporter gene. PKI (shown in blue), which mimics a codon-anticodon duplex, was placed in frame with the coding sequence of Green Fluorescence Protein (GFP). Using this construct, we generated a cDNA library containing the IGR-GFP sequence with the full set of the possible 4096 (64X64) codon-anticodon combinations in frame with PKI. Each IGR-GFP cDNA variant was individualized into droplets (diluted to reach a 20% of occupancy) to limit droplet occupancy by more than one variant. Each variant was first PCR amplified prior to fusing each droplet with another one containing a coupled transcription/translation mixture made of T7 RNA polymerase and rabbit reticulocyte lysate. Upon an hour of incubation at 30°C, droplets were sorted based on their fluorescence. Fluorescent droplets containing active codon-anticodon combinations were recovered, pooled and their cDNA content analyzed by Next Generation Sequencing (NGS). The resulting sequences were compared to NGS sequencing of the starting library for normalization.

Figure 2: Matrix representing the codon-anticodon combinations selected by the microfluidic pipeline.

The sequences of the active codon-anticodon pairs that are efficiently recognized by the ribosome are plotted on a matrix. The 64 codons are represented on the x-axis and 64 anticodons are represented on the y-axis. The nucleotides of the codons are numbered 1, 2 and 3 from 5' to 3'. The nucleotides of the anticodons are numbered 34, 35, 36 from 5' to 3' according to their position in tRNAs. The active codon-anticodon combinations are represented on the matrix by black squares (Watson-Crick pairs are along the diagonal) and by coloured squares for combinations containing mismatches that are parallel to the diagonal. The total number of hits is indicated on the upper right part of the matrix. The number of selected codon-anticodon pairs containing A, C, G and U at position 34 (anticodon) are shown on the right of the matrix. The number of selected codon-anticodon pairs containing A, C, G

and U at position 3 (codon) are shown above the matrix. In each case, the number of hits is decomposed in those along the main diagonal (in black squares) and those off-diagonal (in rainbow squares).

Figure 3: Combinations of codon-anticodon containing Watson-Crick base pairs never isolated through the selection procedure.

(a) Histogram showing the increase in the contribution of G/C base pairs in the selected W-C combinations (see Figure S3 in supplementary material for more detailed distributions). The numbers are normalized to the total number of triplets containing 0 (8), 1 (24), 2 (24), or 3 (8) G/C pairs.

(b) Histogram showing the increase in the contribution of A/U base pairs in the W-C combinations missing from the selection (see Figure S4 in supplementary material for more detailed distributions). The numbers are normalized to the total number of triplets containing 0 (8), 1 (24), 2 (24), or 3 (8) A/U pairs.

(c) Distribution of the missing Watson-Crick combination absent from the selection is plotted on the wheel of the genetic code (blue circles around the third codon base) (56). At the north of the wheel are shown the “strong” or G/C-rich codon-anticodon triplets, at the south the “weak” or A/U-rich codon-anticodon triplets and in the middle the “intermediate” ones as measured by the Turner energy of the helical triplet.

Figure 4: G at position 34 of the anticodon is prone to miscoding in eukaryotes.

(a) The heat map represents, in various eukaryotic genomes, the ratio between the number of genes encoding any of the 64 anticodon combinations and the total number of tRNA genes. The colour code of the heat map is shown on the right, from black for highly represented genes to white for tRNA genes that are absent in genomes. Arrows indicate the suppressor tRNA genes containing anticodons corresponding to the stop codons and tRNA genes containing the anticodons $_{34}GGN_{36}$ and $_{34}GAG_{36}$.

(b) Human tRNA transcripts $tRNA^{Ala,Pro,Thr,Ser,Leu}$ containing $_{34}ANN_{36}$ anticodons and their impossible tRNA (itRNA) counterparts, which contains respectively a single substitution of A at position 34 of the anticodons to G, are introduced into HeLa cells. The histogram represents the Relative Metabolic Activity (RMA) average value measured by WST1 assay for each itRNA transcript (in red) normalized to the corresponding Wt transcript (in orange) (n=9, Statistical Student Test, ns: P-

value>0.05, *: P ≤ 0.05, **: P ≤ 0.01, ***: P ≤ 0.001, ****: P ≤ 0.0001). The error bars represent the standard deviation for each value.

(c) Human $tRNA^{Ala}$ transcripts containing the major determinant $_{3}G\text{-}U_{70}$ for Alanyl-tRNA synthetase with variable anticodon sequences are introduced in Rabbit Reticulocyte Lysates together with a synthetic HA-tagged Renilla reporter mRNA that contains silent mutations at Phenylalanine, Proline, Threonine, Valine, Leucine and Serine codons in order to enrich the proportions of following codons Phenylalanine (UUC), Proline (CCC), Threonine (ACU, ACC), Valine (GUC), Leucine (CUC), Serine (UCC, UCU) according to supplementary figure S9.

(d) The yield of Renilla proteins synthesized in the presence of $tRNA^{Ala}$ transcripts of without transcript (Ø) is evaluated by SDS-PAGE of ^{35}S-Methionine-labelled proteins.

(e) Histogram representing the relative luciferase activities of the synthesized Renilla proteins normalized to the luciferase activity obtained in absence of tRNA transcript (Ø) (n=3, ns: P-value>0.05, **: P ≤ 0.01).

Figure 5: Anticodons with a G34 are prone to miscoding but not when 32-38 can form a Watson-Crick base pair.

Human wild type tRNA transcripts $tRNA^{Ala,Pro,Thr,Leu}$ containing $_{34}ANN_{36}$ anticodons and their impossible tRNA (itRNA) counterparts that contain a single substitution of A at position 34 of the anticodons to G (in red) and double mutants containing an additional single substitution that enables base pairing between 32 and 38 (in green). The $itRNA^{Ala,Pro,Thr,Leu}$ G34 were used as toxicity controls. The three types of tRNA transcripts were introduced into HeLa cells. The histogram represents the Relative Metabolic Activity (RMA) average value measured by WST1 assay for each tRNA transcript normalized to the corresponding Wt transcript (n=6, Statistical Student Test, ns: P-value>0.05, *: P ≤ 0.05, **: P ≤ 0.01, ***: P ≤ 0.001, ****: P ≤ 0.0001). The error bars represent the standard deviation for each value.

Figure 1

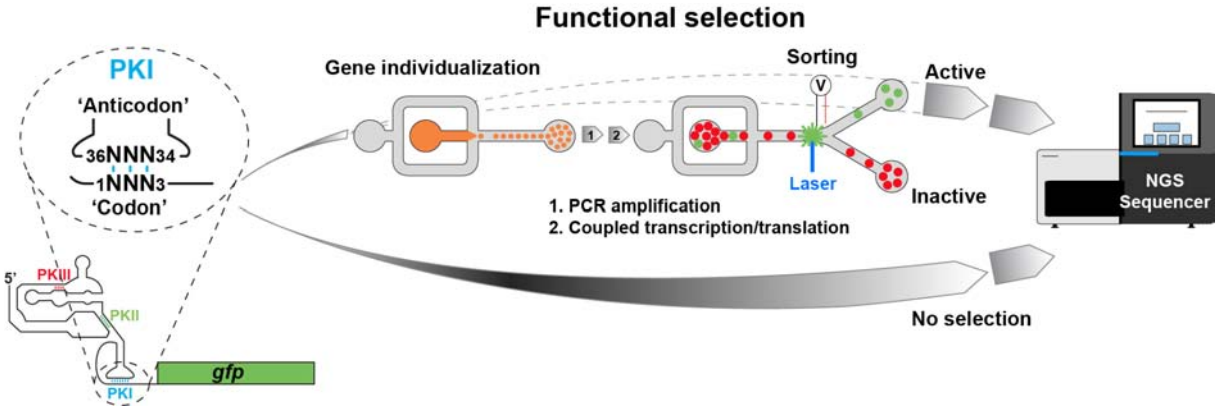
Functional selection
PKI
'Anticodon'
36NNN34
1NNN3
'Codon'
Gene individualization
Sorting
Active
Inactive
Laser
1. PCR amplification
2. Coupled transcription/translation
NGS
Sequencer
No selection
5'
PKIII
PKII
PKI
gfp

Figure 2

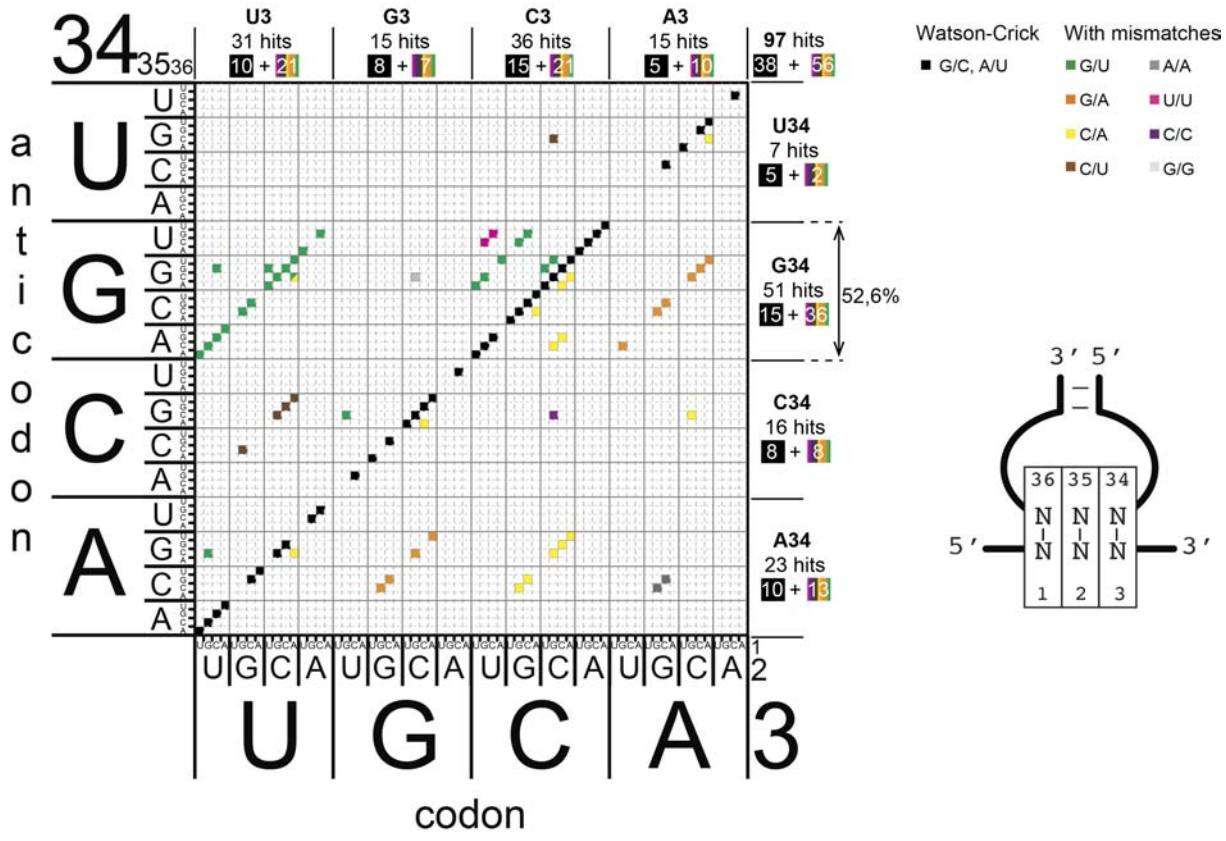
34 35 36
U3
31 hits
10 + 21
G3
15 hits
8 + 7
C3
36 hits
15 + 21
A3
15 hits
5 + 10
97 hits
38 + 56
U34
7 hits
5 + 2
G34
51 hits
15 + 36
52,6%
C34
16 hits
8 + 8
A34
23 hits
10 + 13
anticodon
codon
U G C A
Watson-Crick
G/C, A/U
With mismatches
G/U
A/A
G/A
U/U
C/A
C/C
C/U
G/G
3′ 5′
5′ 3′
36 35 34
N N N
1 2 3

Figure 3

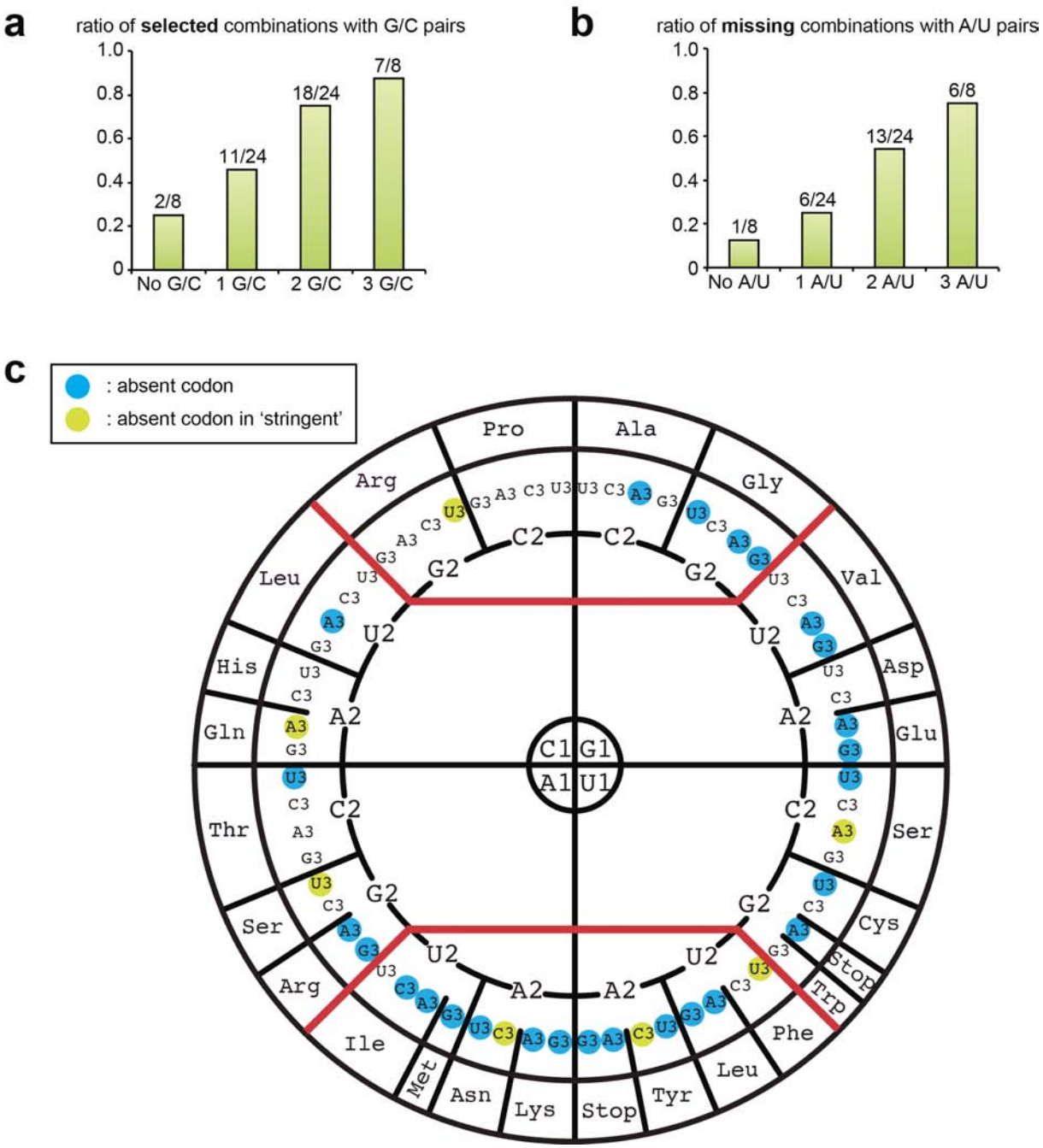
a
ratio of **selected** combinations with G/C pairs
1.0
0.8
0.6
0.4
0.2
0
2/8
11/24
18/24
7/8
No G/C
1 G/C
2 G/C
3 G/C
b
ratio of **missing** combinations with A/U pairs
1.0
0.8
0.6
0.4
0.2
0
1/8
6/24
13/24
6/8
No A/U
1 A/U
2 A/U
3 A/U
c
: absent codon
: absent codon in 'stringent'
Pro
Ala
Arg
Gly
Leu
Val
His
Asp
Gln
Glu
Thr
Ser
Ser
Cys
Arg
Stop
Trp
Ile
Phe
Met
Asn
Lys
Stop
Tyr
Leu
C1 G1
A1 U1
U2
C2
G2
A2

Figure 4

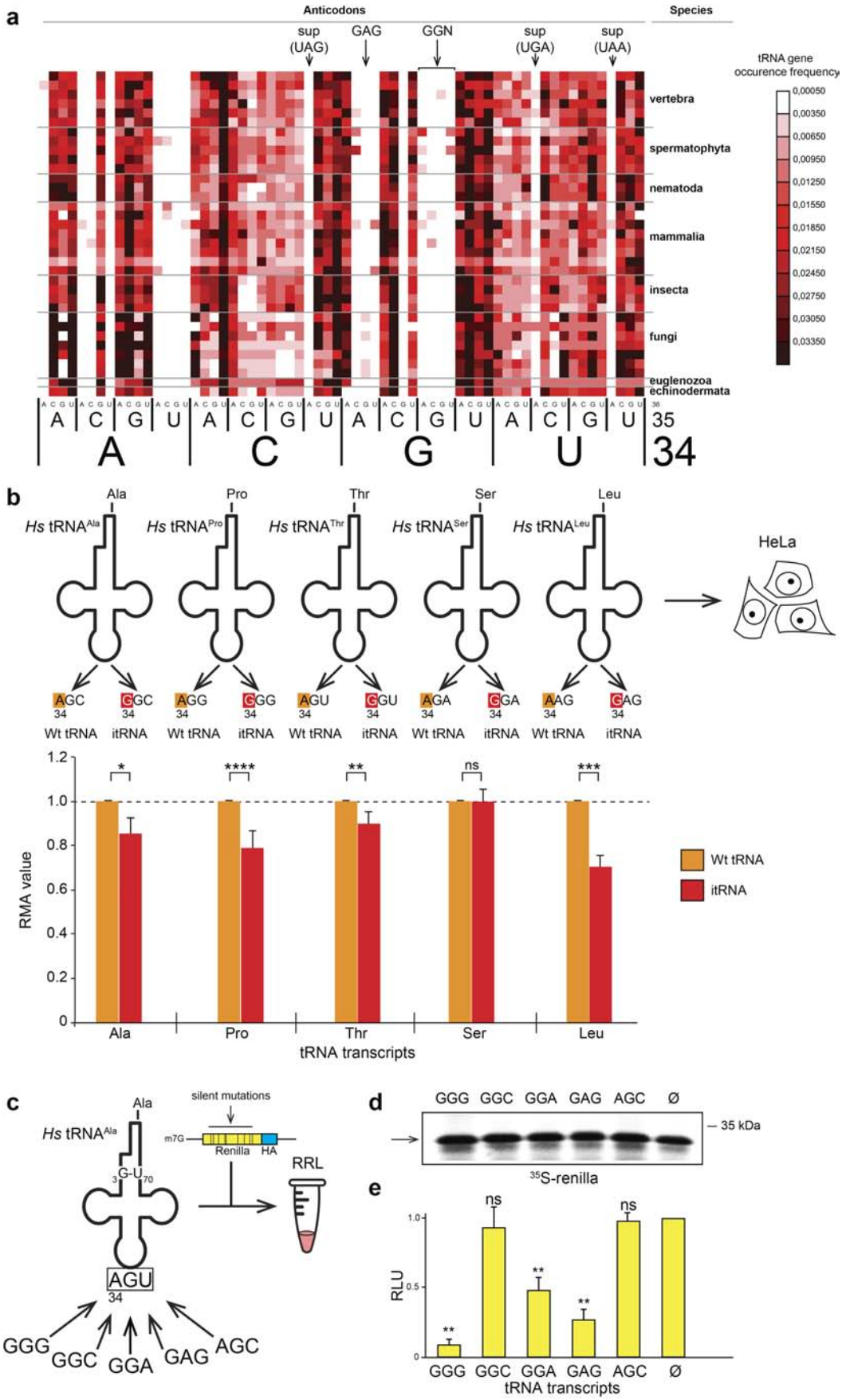
a
Anticodons
Species
sup (UAG)
GAG
GGN
sup (UGA)
sup (UAA)
tRNA gene occurence frequency
0,00050
0,00350
0,00650
0,00950
0,01250
0,01550
0,01850
0,02150
0,02450
0,02750
0,03050
0,03350
vertebra
spermatophyta
nematoda
mammalia
insecta
fungi
euglenozoa
echinodermata
A C G U A C G U A C G U A C G U A C G U A C G U A C G U A C G U A C G U A C G U A C G U A C G U A C G U A C G U 35
A C G U A C G U A C G U A C G U A C G U A C G U A C G U A C G U A C G U A C G U A C G U A C G U A C G U 36
A C G U 34
b
Ala
Pro
Thr
Ser
Leu
Hs tRNAAla
Hs tRNAPro
Hs tRNAThr
Hs tRNASer
Hs tRNALeu
HeLa
AGC 34 Wt tRNA
GGC 34 itRNA
AGG 34 Wt tRNA
GGG 34 itRNA
AGU 34 Wt tRNA
GGU 34 itRNA
AGA 34 Wt tRNA
GGA 34 itRNA
AAG 34 Wt tRNA
GAG 34 itRNA
RMA value
1.2
1.0
0.8
0.6
0.4
0.2
0
*
****
**
ns
***
Wt tRNA
itRNA
Ala
Pro
Thr
Ser
Leu
tRNA transcripts
c
Ala
Hs tRNAAla
G-U
3
70
silent mutations
m7G
Renilla
HA
RRL
AGU
34
GGG
GGC
GGA
GAG
AGC
d
GGG GGC GGA GAG AGC Ø
35 kDa
35S-renilla
e
RLU
1.0
0.5
0
ns
**
**
**
ns
GGG GGC GGA GAG AGC Ø
tRNA transcripts

Figure 5

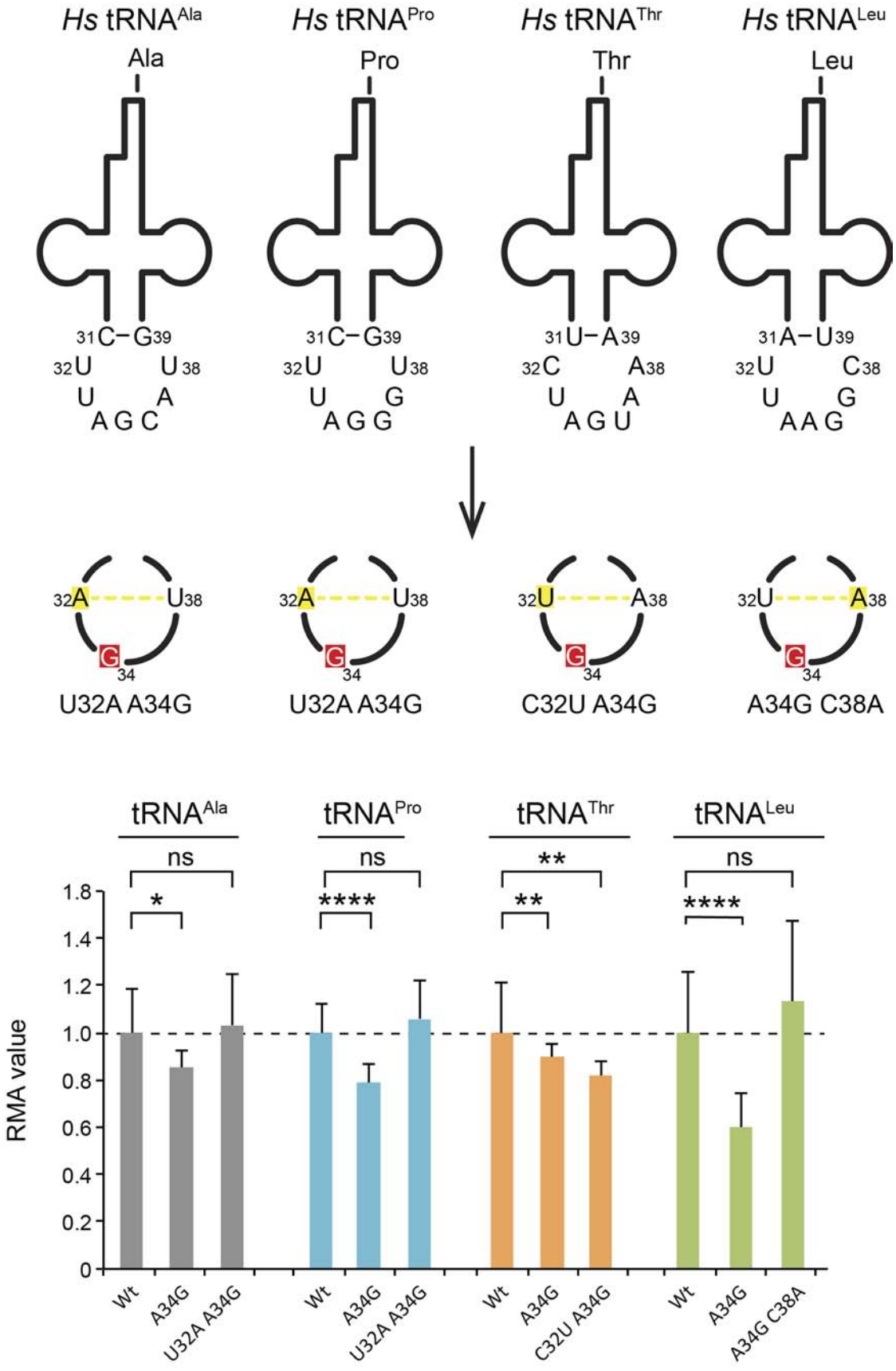
Hs tRNAAla
Ala
31C–G39
32U U38
U A
A G C
Hs tRNAPro
Pro
31C–G39
32U U38
U G
A G G
Hs tRNAThr
Thr
31U–A39
32C A38
U A
A G U
Hs tRNALeu
Leu
31A–U39
32U C38
U G
A A G
32A U38
G 34
U32A A34G
32A U38
G 34
U32A A34G
32U A38
G 34
C32U A34G
32U A38
G 34
A34G C38A
tRNAAla
tRNAPro
tRNAThr
tRNALeu
ns
*
ns
****
**
**
ns
****
RMA value
1.8
1.4
1.2
1.0
0.8
0.6
0.4
0.2
0
Wt
A34G
U32A A34G
Wt
A34G
U32A A34G
Wt
A34G
C32U A34G
Wt
A34G
A34G C38A

Supplementary information

Captions for supplementary figures

Figure S1: PKI structurally and functionally mimics a codon-anticodon helix
Comparison of the base pairing between the tRNA anticodon numbered 34, 35, 36 with a cognate codon numbered 1, 2, 3 shown on the left and the pseudoknot PKI from CrPV Intergenic IRES. Structure of the Anticodon Stem Loop or ASL (in orange) base paired to a cognate codon in the A site of the ribosome (on the left) and structure of PKI in the A site of the ribosome (on the right) are represented from respectively X-ray (pdb:5e81) (16) and CryoEM (pdb: 5it9) (33) molecular models. The tRNA anticodon part is in red and the mRNA codon part in cyan. In the IRES structure, the 5'-end of the "mRNA" continues to pair with the "anticodon 37 and 38". A library containing the 4096 codon-anticodon combinations in the frame of PKI was generated.

Figure S2: Ultrahigh-throughput screening of randomized IRES gene libraries.
(a) Schematic of the droplet-based microfluidic screening pipeline. The screening pipeline operates in three main steps. First, the genes of the library are diluted into a PCR mixture prior to being individualized into small picoliter-sized water-in-oil droplets (left device). The emulsion is collected off-chip into a conventional PCR tube and the whole emulsion is thermocycled into a regular thermocycler. Next, the amplified DNA-containing droplets (orange) are reinjected into a fusion device (middle device) and synchronized with on-chip generated droplets (red) containing an *in vitro* expression mixture (a Rabbit Reticulocyte Lysate supplemented in T7 RNA polymerase in this study). Both sets of droplets are synchronized, fused by an electric field and collected off-chip. Genes are then expressed during an off-chip incubation step prior to reinjecting the droplets into a last device (right device) aiming at analyzing droplets fluorescence and sorting them accordingly. **(b)** Occurrence frequency matrix of the 4096 variants contained in the starting gene library. The occurrence frequency has been calculated for each variant contained in the starting library and the value was color-coded accordingly. The ~ 6-fold occurrence difference between the most and the least represented variant is supportive of a generally unbiased the library and confirmed that a ~ 37-fold coverage was enough to see

each variant during the first rounds of screening. **(c)** Representation of the evenness of the variants contained in the starting library. Sequences were ordered and numbered according to their occurrence in the library (a sequence ID inversely proportional to the occurrence was attributed each sequence) prior to being plotted as a function of their cumulative occurrence. The straight alignment of the point is indicative of an overall even representation of the different variants. **(d)** GFP fluorescence profile of the droplets from the two replicates of the experiment. In each experiment, the dashed line indicates the lower limit of the sorting gate. The sorting gate was set such that every droplet with a fluorescence detached from the negative population was recovered. **(e)** Representation evenness of the variants selected in each replicate. Sequences were ordered and numbered according to their occurrence in the library (a sequence ID inversely proportional to the occurrence was attributed each sequence) prior to being plotted as a function of their cumulative occurrence. Sequences corresponding to molecules initially individualized and amplified several hundreds of times in droplets are expected to be over-represented in comparison to those coming from a rare mutation event during PCR or from a sequencing error. Therefore, whereas the formers are expected to accumulate at a high, the latter should accumulate more slowly and a biphasic curve like those observed here is expected. Consequently, the breakpoint at the junction of both curves corresponds to the threshold between the relevant sequences (signal) and the non-relevant ones (noise). The Venn diagram represents the combinations that are present in both replicates.

Figure S3: Combinations of codon-anticodon containing Watson-Crick base pairs that are selected

The combinations are ranked according the 3-34 pair and their proportion is shown in parentheses. Interestingly, the combinations Y3/R34 are two times more frequent than the combinations R3/Y34. The amino acids coded by the corresponding codons are shown under each combination. No combination was selected for Methionine, Glutamic acid, Lysine and the three stop codons.

Figure S4: Combinations of codon-anticodon containing Watson-Crick base pairs that are not selected

The combinations are ranked according the position of A/U base pairs (shown in blue). Start (green dot) and stop codons (red dots) are indicated. The proportion of each category is shown under the figure. The two pie charts represent the proportion of nucleotides at position 34 and 3 in these missing combinations.

Figure S5: Combinations of selected codon-anticodon containing Watson-Crick base pairs with one or two mismatches

(a) The codon-anticodon combinations are listed according to the position of the mismatches. There are 56 combinations with one mismatch and three with two. The mismatches are colour-coded (G/U in green, G/A in orange, C/A in yellow, C/U in brown, A-A in dark grey, U-U in purple and G-G in light grey). The proportion and position of each mismatch are summarized at the bottom. About 2/3 of mismatches occur at the third “wobble” position and the most frequent are G/U (12), G/A (10), C/A (6) and C/U (5).

(b) The histogram represents the number of mismatches obtained for each of the three positions of the codon. The pie charts represent the proportion of each of the four nucleotides at position 34 in the codon-anticodon combinations containing mismatches at position 1 and 2, and at position 3 of the codon.

(c) The histograms represent the total number of each type of mismatch at the three positions of the codon.

Figure S6: Combinations of selected codon-anticodon interacting with one or two mismatches.

(a) The histogram represents the number of G/U (green), C/A (yellow), G/A (orange) and U/C mismatches (brown) found in each of the 3 positions of the codon. Striped bars represent the orientations 1-36, 2-35 and 3-34 and full bars represent the opposite orientations. The pie charts represent the proportion of each orientation in the 3 positions of the codon.

(b) The histogram represents the relative Renilla luciferase activity obtained with PKI in frame of a Renilla luciferase reporter with several codon-anticodon combinations. Combinations that were selected through the microfluidic pipeline are indicated by (+) and combinations that were not selected are indicated by (-).

(c) Experimental validation of the preferred orientation of G/U mismatches at the position 3 of the codon. The histogram represents the relative Renilla luciferase

activities of codon-anticodon combinations in PK1 with G/U mismatches in both orientation at the three positions of the codons and in frame with a Renilla coding sequence.

Figure S7: Second selection on the combinations in 'stringent' conditions.
(a) GFP fluorescence profile of the droplets from the two replicates of the selection in stringent conditions. In each experiment, the dashed line indicates the lower limit of the sorting gate. Representation evenness of the variants selected in each replicate is shown below the fluorescent profiles. Sequences were ordered and numbered according to their occurrence in the library (a sequence ID inversely proportional to the occurrence was attributed each sequence) prior to being plotted as a function of their cumulative occurrence. The straight alignment of the point is indicative of an overall even representation of the different variants. The Venn diagram represents the combinations that are present in both replicates. **(b)** The sequences of the active codon-anticodon pairs that are efficiently recognized by the ribosome in 'stringent' conditions are plotted on a matrix. The 64 codons are represented on the x-axis and 64 anticodons are represented on the y-axis. The nucleotides of the codons are numbered 1, 2 and 3 from 5' to 3'. The nucleotides of the anticodons are numbered 34, 35, 36 from 5' to 3' according to their position in tRNAs. The active codon-anticodon combinations are represented on the matrix by black squares (Watson-Crick pairs are along the diagonal) and by coloured squares for combinations containing mismatches that are parallel to the diagonal. The total number of hits is indicated on the upper right part of the matrix. The number of selected codon-anticodon pairs containing A, C, G and U at position 34 (anticodon) are shown on the right of the matrix. The number of selected codon-anticodon pairs containing A, C, G and U at position 3 (codon) are shown above the matrix. **(c**) Histogram representing the number of mismatches obtained in each of the three positions of the codons. The proportion of each of the four nucleotides at position 34 is shown in the pie charts for mismatches at positions 1 and 2 and at position 3.

Figure S8: The anticodons with a G34 are prone to miscoding
The 51 active codon-anticodon pairs containing G34 that are selected in the 'Relaxed' selection procedure are plotted on the matrix. Combinations containing

Watson-Crick base pairs are represented by black squares (15) and combinations containing mismatches (36) are highlighted using coloured squares according to the figure legend. The combinations that would lead to miscoding (and not G/U wobbling) are circled. The codons that are incorrectly decoded are indicated above the matrix and the anticodons that induce miscoding are shown on the right. The resulting miscoding events would, in a natural system, induce incorporations of non-cognate amino acids (in black) instead of the cognate amino acids (in red). An asterisk indicates the miscoding combination (Pro>Ser or $_{1}CCC_{3}/_{34}GGA_{36}$) that has been validated with a reporter gene by Mass Spectrometry (see S10).

Figure S9: Evolutionary clearance of G34 containing tRNAs in eukaryotic tRNAs of 3- and 4-codon boxes.

The heat map represents the ratio of the number of each of the putative tRNA gene corresponding to the 64 anticodons divided by the total number of tRNA genes in various eukaryotic genomes. The colour code is indicated at the bottom of the figure from black for abundant tRNA genes to white for tRNA genes that are absent from eukaryotic genomes. The species are indicated at the top of the figure and the anticodon for each tRNA gene, the corresponding codon and the amino acid identity are shown in the table on the right part of the figure. The orange boxes indicate that the tRNA genes containing anticodon starting with an A at position 34 are rare or absent. The yellow boxes indicate that the tRNA genes containing an anticodon starting with a G at position 34 are rare or absent. The cartoon on the right part summarizes the results on the heat map. In eukaryotes, the A34-containing tRNA genes were cleared throughout evolution in 2-box tRNA sets and the G34-containing tRNA genes have been cleared in 3- and 4-box tRNA sets (with the exception of Gly, a 4-box tRNA in which A34 has been cleared to favour G34). In eukaryotes, A34 is modified into I34; the clearance of A34 in 2-codon boxes results from the miscoding potential of I (that can pair with C, U, and A)(59).

Figure S10: Anticodons containing G34 do promote miscoding in Rabbit Reticulocyte Lysates.

The Renilla luciferase protein produced in rabbit reticulocyte lysate in the presence of *Homo sapiens* $tRNA^{Ala}_{GNN}$ transcripts and synthetic Renilla mRNA was purified via its C-terminal HA-tag, digested by trypsin and analysed by Mass Spectrometry. **(a)**

Mass Spectrometry analysis of the peptide sequence from Renilla luciferase protein produced in presence of *Homo sapiens* $tRNA^{Ala}_{GGA}$. The upper panel represents the wild-type peptide ($_{253}$MFIESDPGFFSNAIVEGAK$_{271}$) containing the expected Serine residue highlighted in yellow at the position of the Serine UCC codon inserted by endogenous $tRNA^{Ser}$. The lower panel shows the same peptide where the Serine was substituted with an Alanine residue (also in yellow) by the exogenous *Homo sapiens* $tRNA^{Ala}_{GGA}$ transcript confirming that this synthetic chimera is efficiently alanylated by endogenous AlaRS and picked up by ribosomes available in Rabbit Reticulocyte Lysates. **(b)** Mass Spectrometry analysis of the same reporter peptide. The upper panel shows the sequence of the peptide containing the expected Proline residue highlighted in yellow at the position of the Proline CCC codon inserted by endogenous $tRNA^{Pro}$. The lower panel shows the peptide where the Proline was substituted with Alanine (also in yellow) by the exogenous *Homo sapiens* $tRNA^{Ala}_{GGA}$ confirming that this anticodon supports miscoding when a C-A mismatch is present at the first position of the codon.

Figure S1

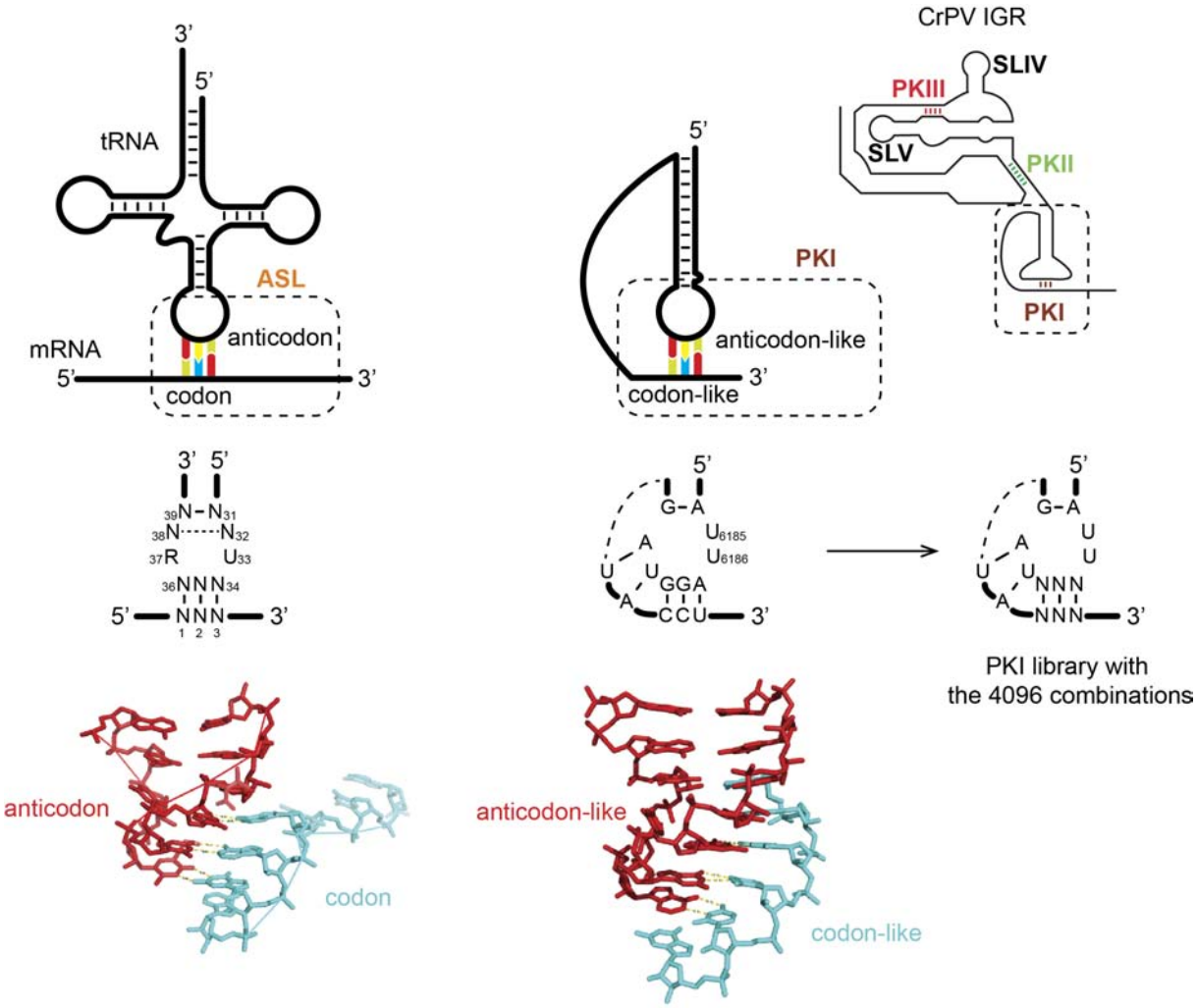
3'
5'
tRNA
ASL
anticodon
mRNA
5'
3'
codon
CrPV IGR
SLIV
PKIII
SLV
PKII
PKI
5'
PKI
anticodon-like
3'
codon-like
3' 5'
39N–N31
38N·····N32
37R U33
36NNN34
5'—NNN—3'
1 2 3
5'
G–A
A U6185
U6186
U U
GGA
A CCU—3'
5'
G–A
A U
U U
U NNN
A
NNN—3'
PKI library with
the 4096 combinations
anticodon
codon
anticodon-like
codon-like

Figure S2

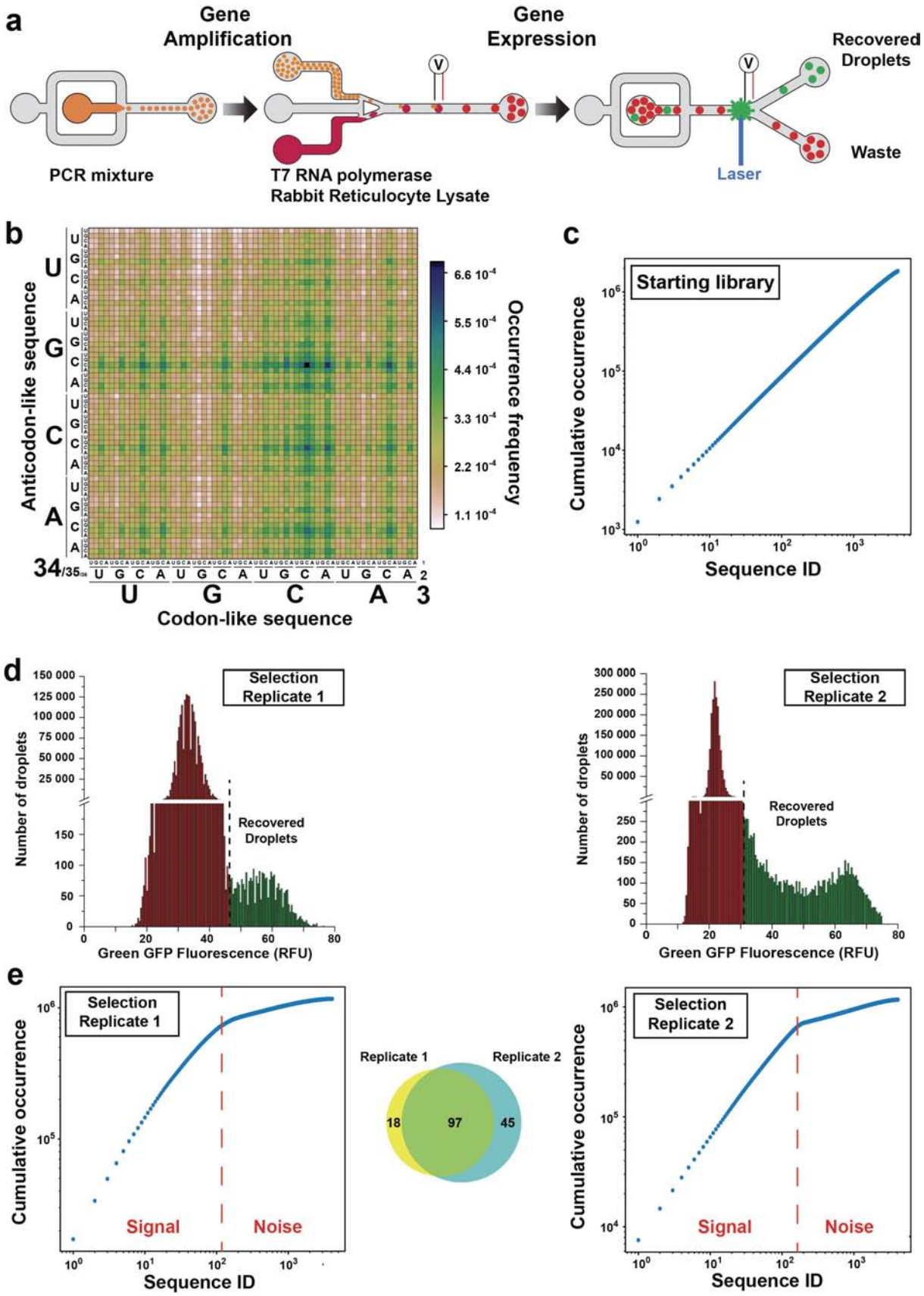
a
Gene Amplification
Gene Expression
Recovered Droplets
Waste
PCR mixture
T7 RNA polymerase
Rabbit Reticulocyte Lysate
Laser
b
Anticodon-like sequence
Codon-like sequence
Occurrence frequency
c
Starting library
Cumulative occurrence
Sequence ID
d
Selection Replicate 1
Selection Replicate 2
Number of droplets
Recovered Droplets
Green GFP Fluorescence (RFU)
e
Selection Replicate 1
Selection Replicate 2
Cumulative occurrence
Signal
Noise
Sequence ID
Replicate 1
Replicate 2
18
97
45

Figure S3

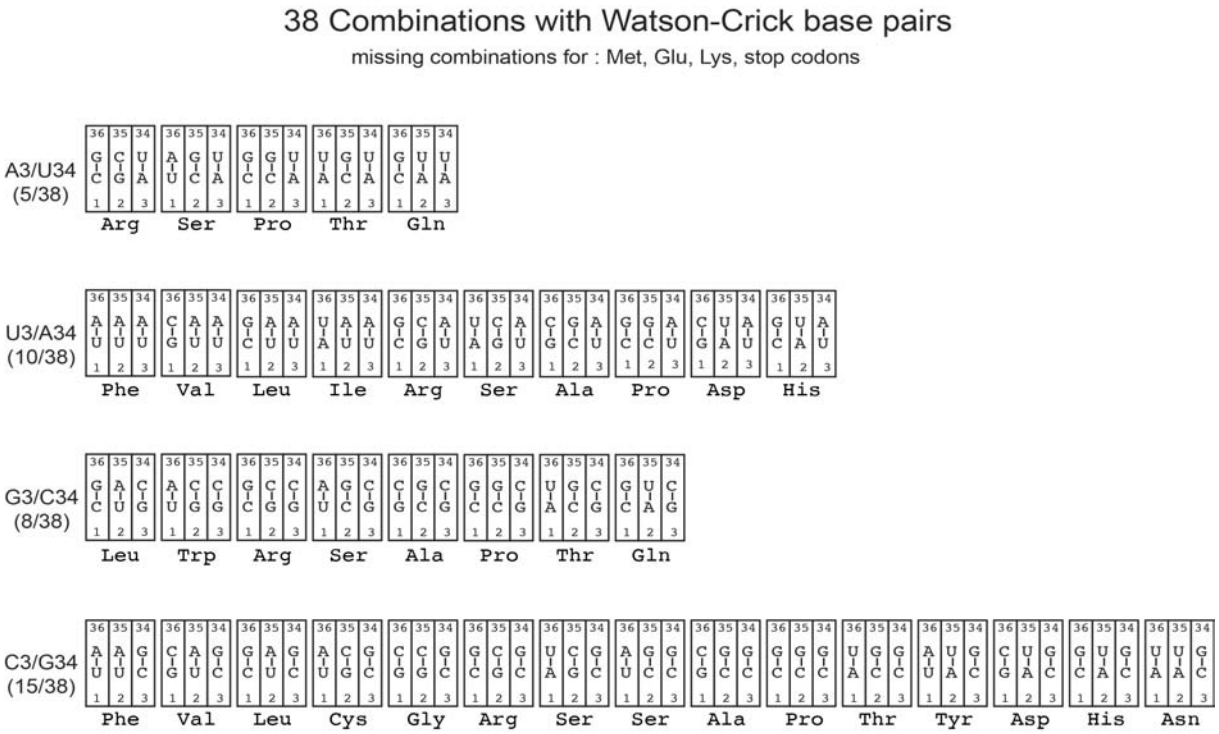
38 Combinations with Watson-Crick base pairs
missing combinations for : Met, Glu, Lys, stop codons
A3/U34 (5/38)
Arg Ser Pro Thr Gln
U3/A34 (10/38)
Phe Val Leu Ile Arg Ser Ala Pro Asp His
G3/C34 (8/38)
Leu Trp Arg Ser Ala Pro Thr Gln
C3/G34 (15/38)
Phe Val Leu Cys Gly Arg Ser Ser Ala Pro Thr Tyr Asp His Asn

Figure S4

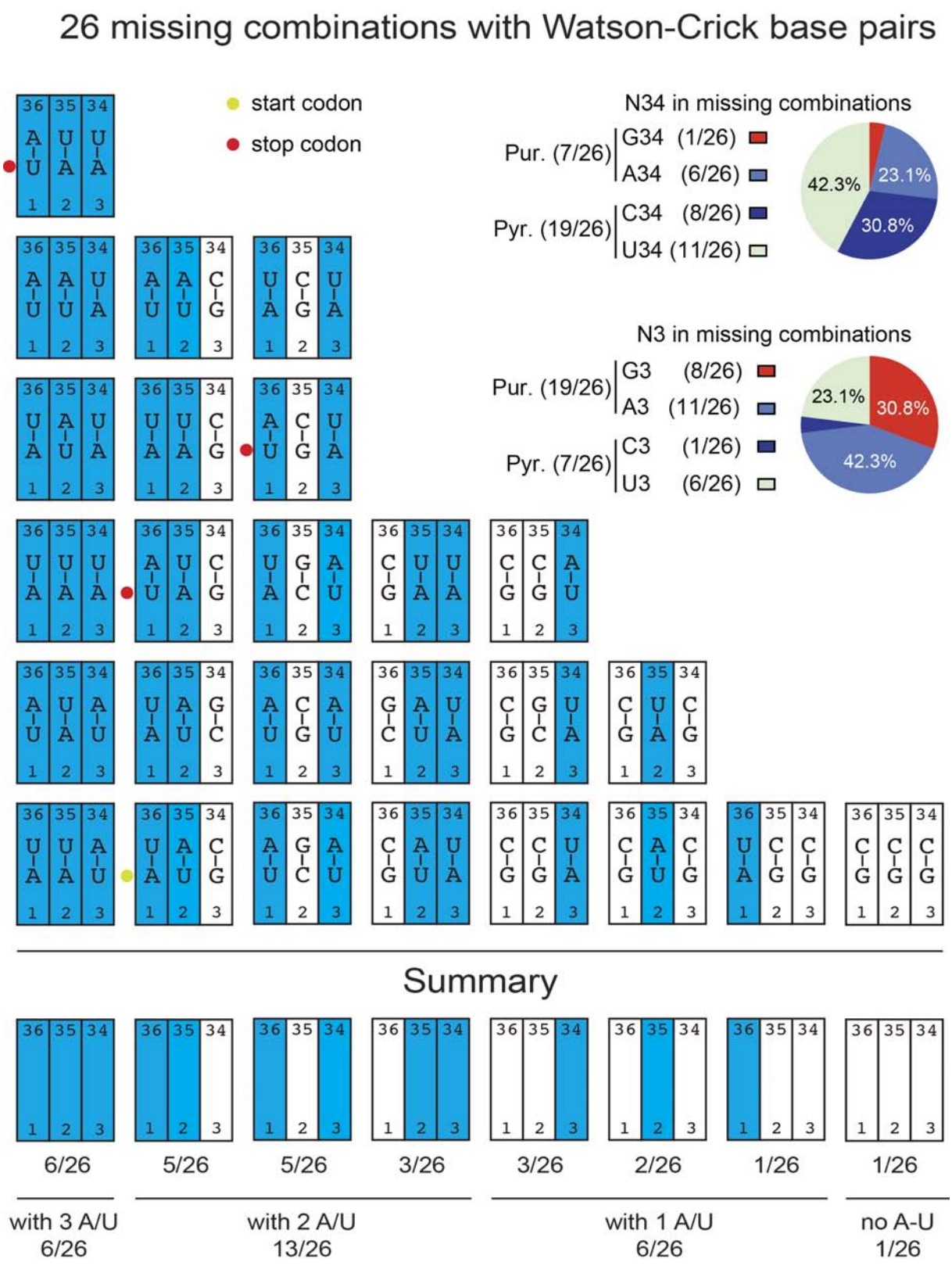
26 missing combinations with Watson-Crick base pairs
start codon
stop codon
N34 in missing combinations
Pur. (7/26)
G34 (1/26)
A34 (6/26)
Pyr. (19/26)
C34 (8/26)
U34 (11/26)
42.3%
23.1%
30.8%
N3 in missing combinations
Pur. (19/26)
G3 (8/26)
A3 (11/26)
Pyr. (7/26)
C3 (1/26)
U3 (6/26)
23.1%
30.8%
42.3%
Summary
6/26
5/26
5/26
3/26
3/26
2/26
1/26
1/26
with 3 A/U
6/26
with 2 A/U
13/26
with 1 A/U
6/26
no A-U
1/26

Figure S5a

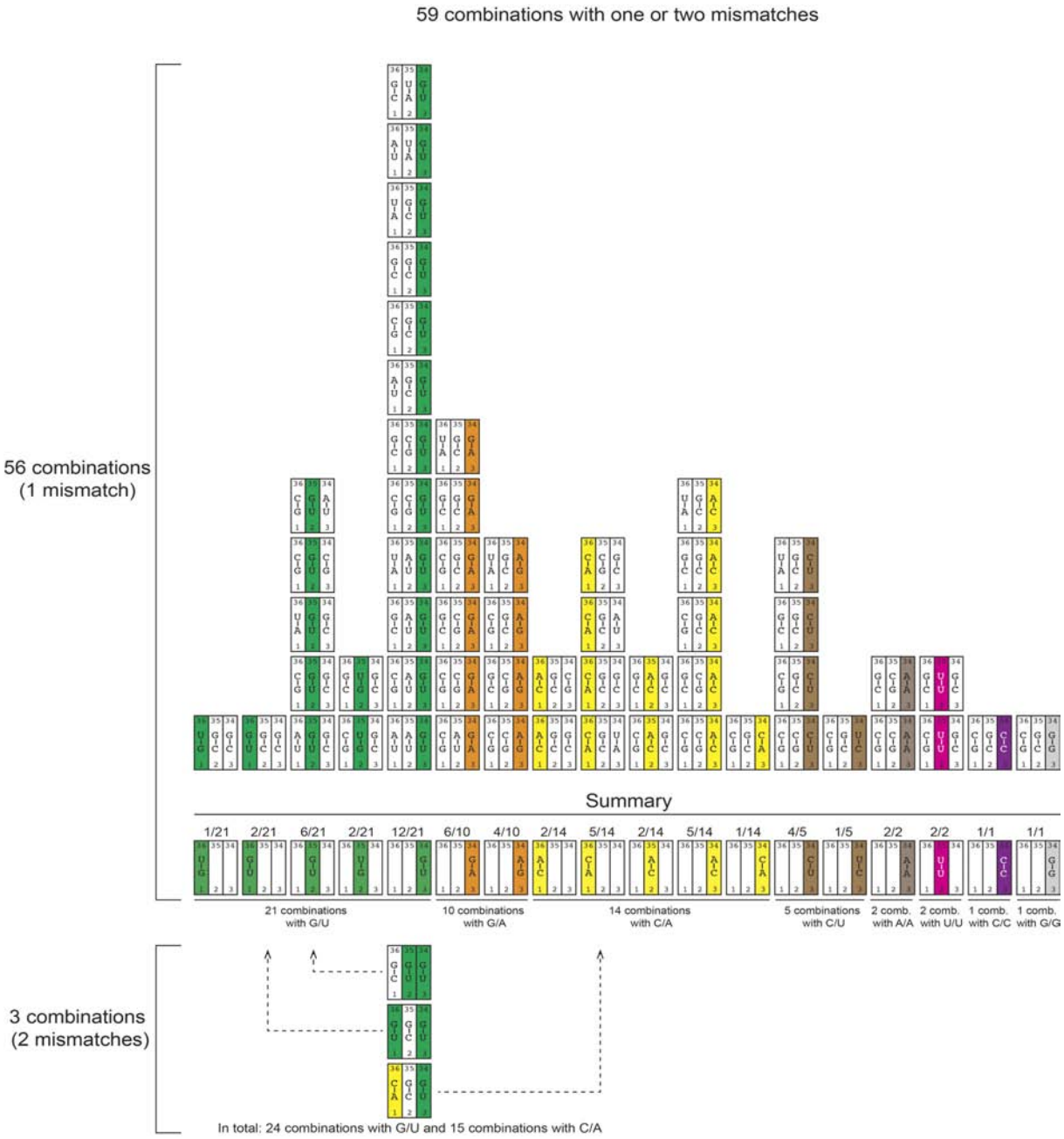
59 combinations with one or two mismatches
56 combinations
(1 mismatch)
Summary
1/21
2/21
6/21
2/21
12/21
6/10
4/10
2/14
5/14
2/14
5/14
1/14
4/5
1/5
2/2
2/2
1/1
1/1
21 combinations with G/U
10 combinations with G/A
14 combinations with C/A
5 combinations with C/U
2 comb. with A/A
2 comb. with U/U
1 comb. with C/C
1 comb. with G/G
3 combinations
(2 mismatches)
In total: 24 combinations with G/U and 15 combinations with C/A

Figure S5

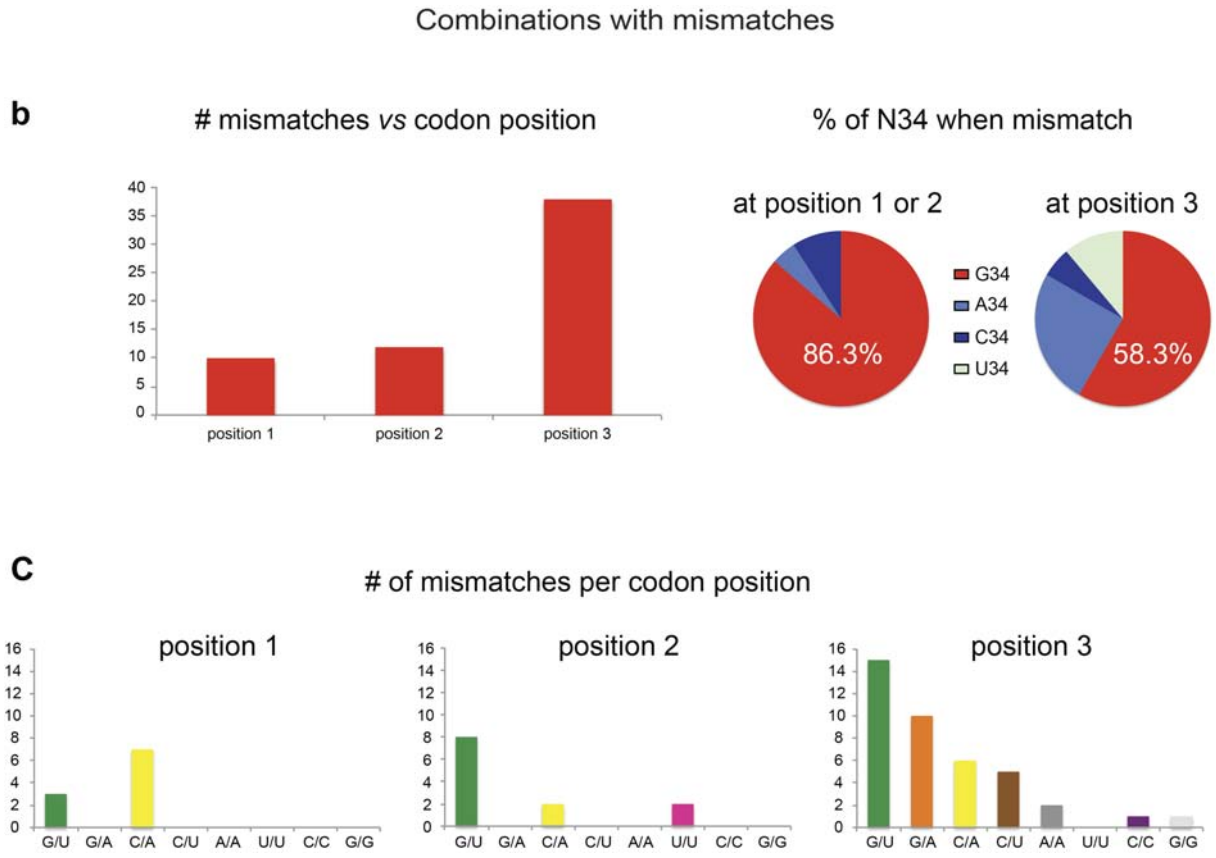
Combinations with mismatches
b
mismatches vs codon position
40
35
30
25
20
15
10
5
0
position 1
position 2
position 3
% of N34 when mismatch
at position 1 or 2
86.3%
G34
A34
C34
U34
at position 3
58.3%
c
# of mismatches per codon position
position 1
position 2
position 3
16
14
12
10
8
6
4
2
0
G/U G/A C/A C/U A/A U/U C/C G/G

Figure S6a

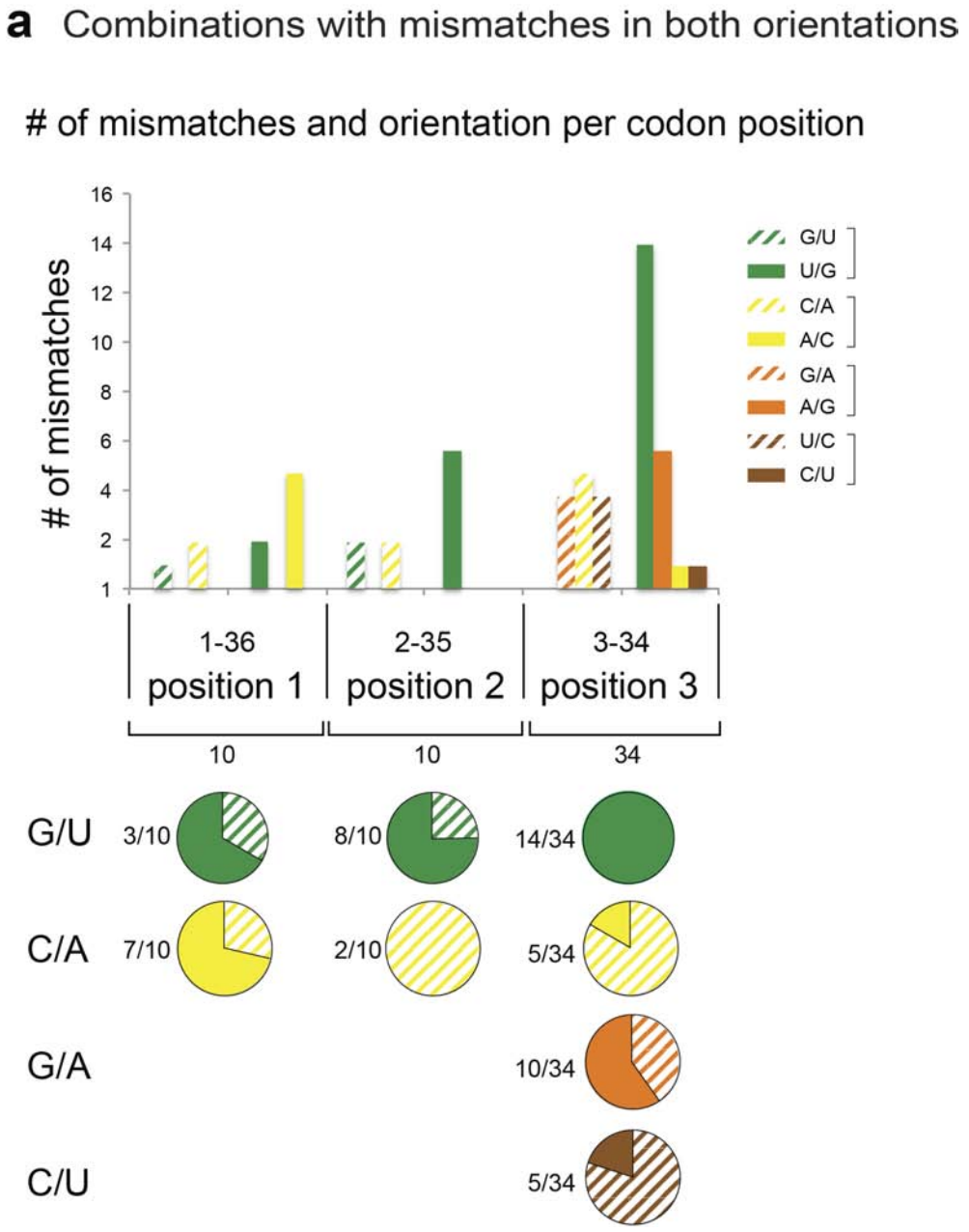
a Combinations with mismatches in both orientations
# of mismatches and orientation per codon position
# of mismatches
16
14
12
10
8
6
4
2
1
G/U
U/G
C/A
A/C
G/A
A/G
U/C
C/U
1-36
position 1
2-35
position 2
3-34
position 3
10
10
34
G/U
3/10
8/10
14/34
C/A
7/10
2/10
5/34
G/A
10/34
C/U
5/34

Figure S6b-c

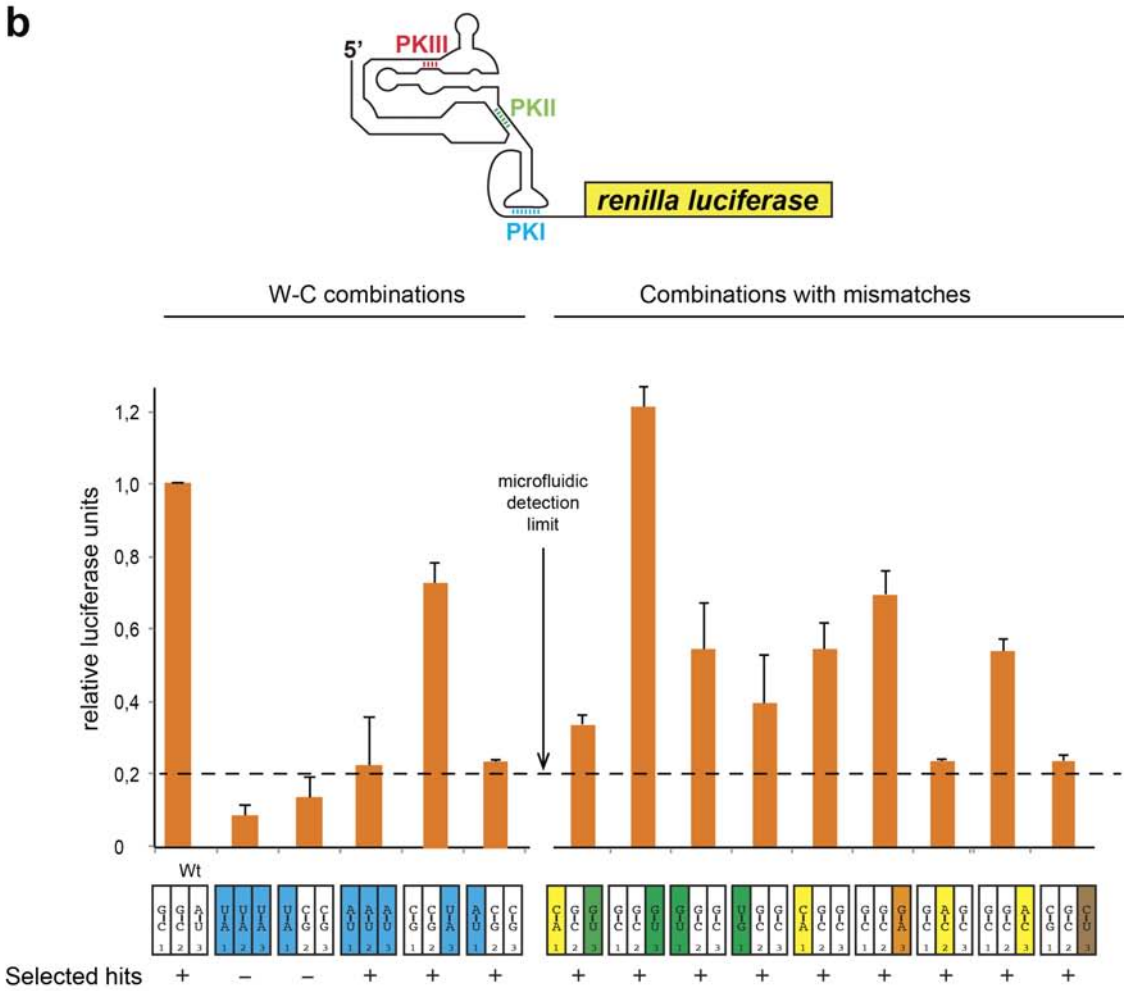
b
5'
PKIII
PKII
PKI
renilla luciferase
W-C combinations
Combinations with mismatches
relative luciferase units
microfluidic detection limit
Wt
Selected hits

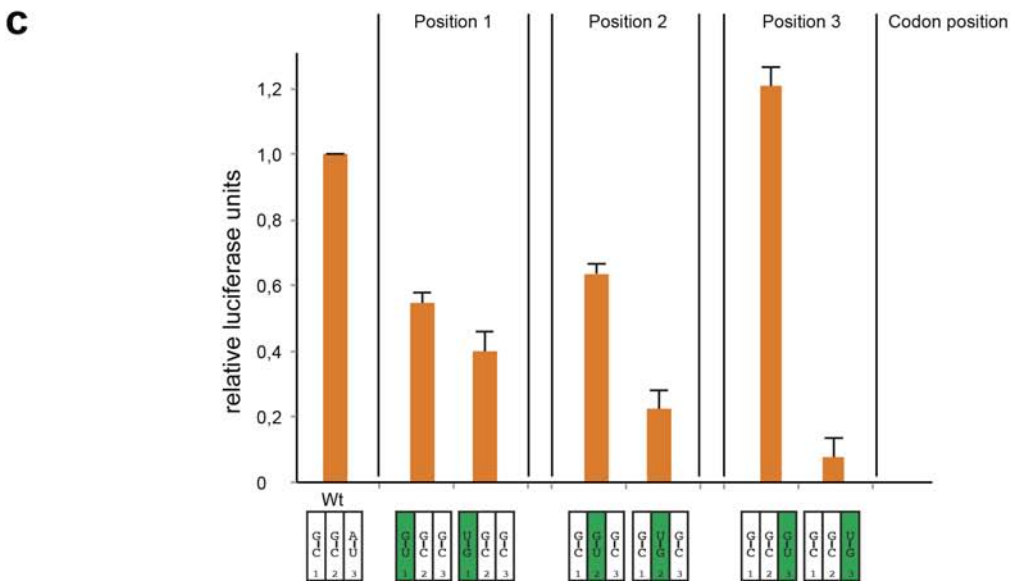
c
Position 1
Position 2
Position 3
Codon position
relative luciferase units
Wt

Figure S7

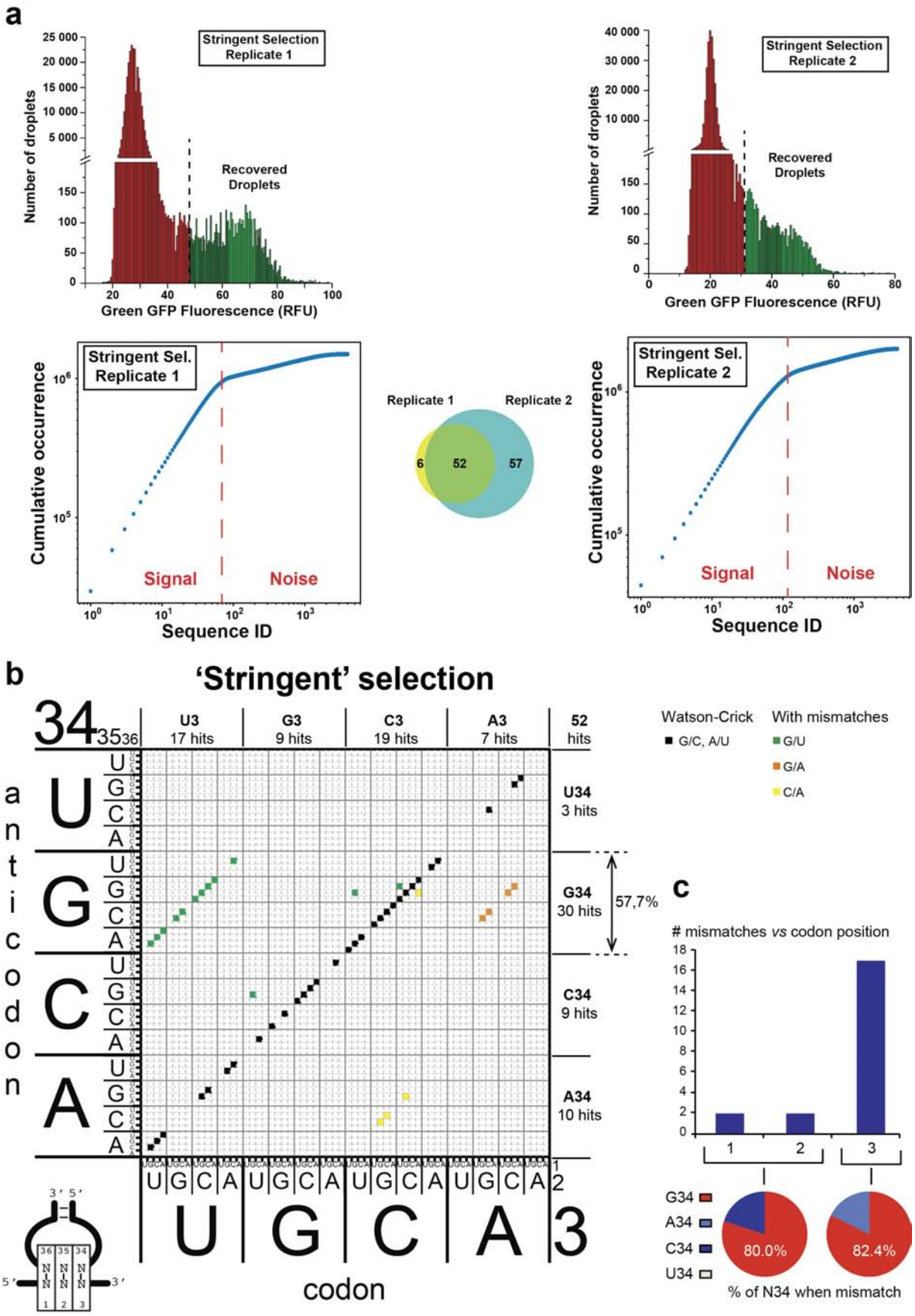
a
Stringent Selection Replicate 1
Number of droplets
Recovered Droplets
Green GFP Fluorescence (RFU)
Stringent Selection Replicate 2
Number of droplets
Recovered Droplets
Green GFP Fluorescence (RFU)
Stringent Sel. Replicate 1
Cumulative occurrence
Signal
Noise
Sequence ID
Replicate 1
Replicate 2
6
52
57
Stringent Sel. Replicate 2
Cumulative occurrence
Signal
Noise
Sequence ID
b
'Stringent' selection
34
35 36
U3 17 hits
G3 9 hits
C3 19 hits
A3 7 hits
52 hits
anticodon
U34 3 hits
G34 30 hits
57,7%
C34 9 hits
A34 10 hits
codon
Watson-Crick
G/C, A/U
With mismatches
G/U
G/A
C/A
c
mismatches vs codon position
G34
A34
C34
U34
80.0%
82.4%
% of N34 when mismatch

Figure S8

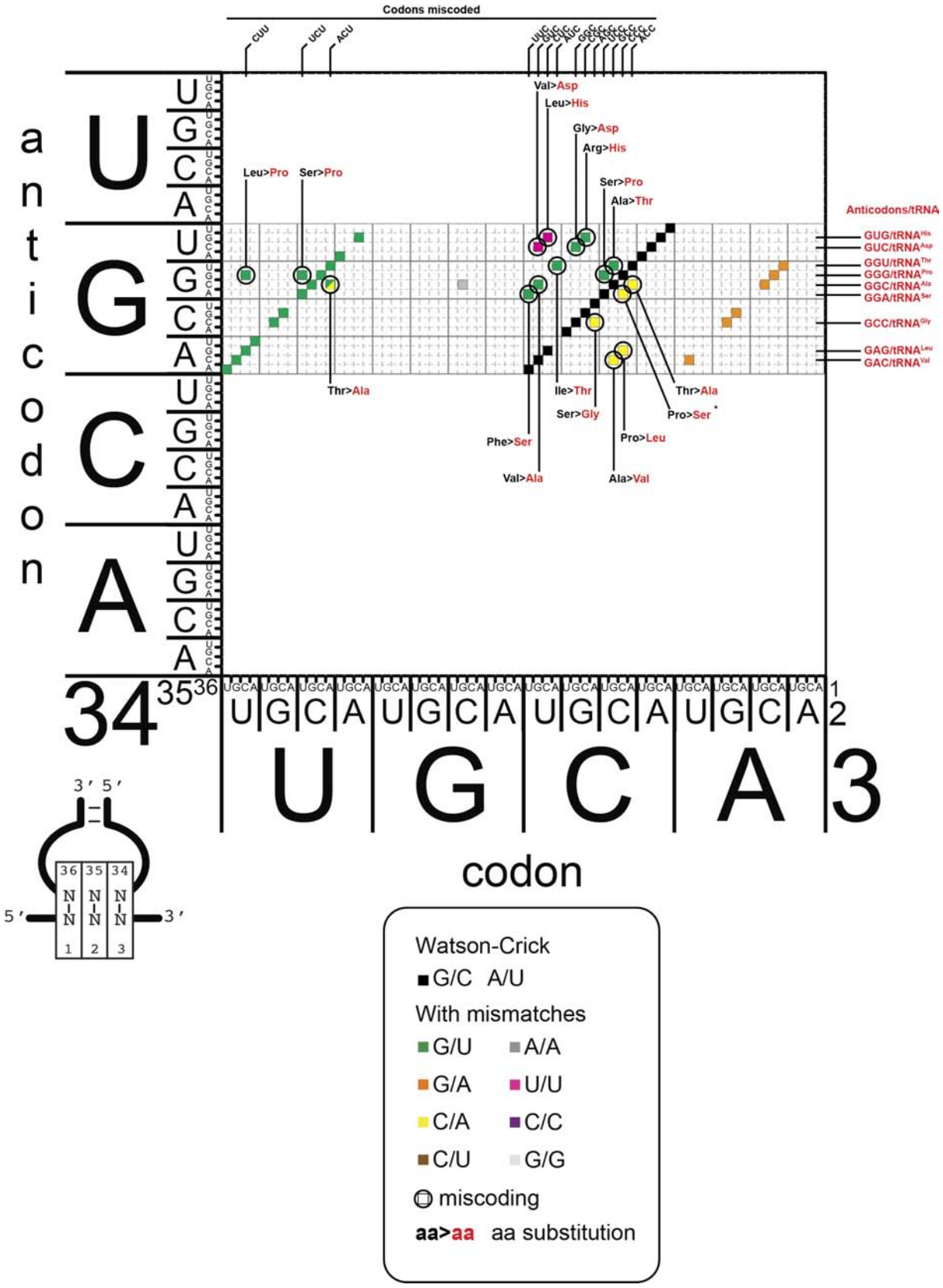
Codons miscoded
CUU
UCU
ACU
anticodon
codon
Val>Asp
Leu>His
Gly>Asp
Arg>His
Leu>Pro
Ser>Pro
Ser>Pro
Ala>Thr
Thr>Ala
Ile>Thr
Ser>Gly
Thr>Ala
Pro>Ser *
Phe>Ser
Pro>Leu
Val>Ala
Ala>Val
Anticodons/tRNA
GUG/tRNA His
GUC/tRNA Asp
GGU/tRNA Thr
GGG/tRNA Pro
GGC/tRNA Ala
GGA/tRNA Ser
GCC/tRNA Gly
GAG/tRNA Leu
GAC/tRNA Val
Watson-Crick
G/C A/U
With mismatches
G/U
A/A
G/A
U/U
C/A
C/C
C/U
G/G
miscoding
aa>aa aa substitution

Figure S9

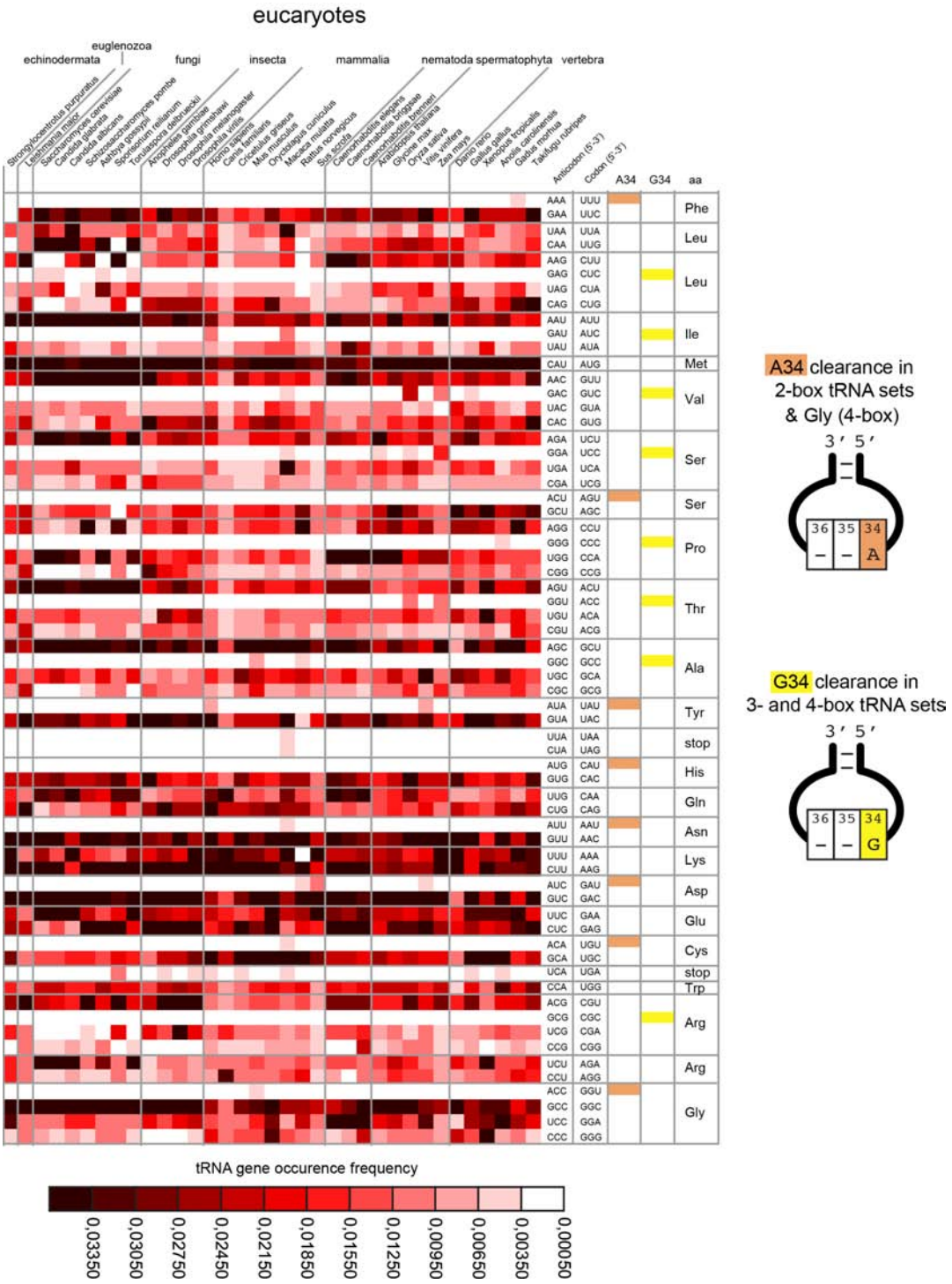
eucaryotes
euglenozoa
echinodermata
fungi
insecta
mammalia
nematoda
spermatophyta
vertebra
Strongylocentrotus purpuratus
Leishmania major
Saccharomyces cerevisiae
Candida glabrata
Candida albicans
Schizosaccharomyces pombe
Ashbya gossypii
Sporisorium reilianum
Torulaspora delbrueckii
Anopheles gambiae
Drosophila grimshawi
Drosophila melanogaster
Drosophila virilis
Homo sapiens
Canis familiaris
Cricetulus griseus
Mus musculus
Oryctolagus cuniculus
Macaca mulatta
Rattus norvegicus
Sus scrofa
Caenorhabditis elegans
Caenorhabditis briggsae
Caenorhabditis remanei
Arabidopsis thaliana
Glycine max
Oryza sativa
Vitis vinifera
Zea mays
Danio rerio
Gallus gallus
Xenopus tropicalis
Anolis carolinensis
Gadus morhua
Takifugu rubripes
Anticodon (5'-3')
Codon (5'-3')
A34
G34
aa
AAA UUU Phe
GAA UUC
UAA UUA Leu
CAA UUG
AAG CUU Leu
GAG CUC
UAG CUA
CAG CUG
AAU AUU Ile
GAU AUC
UAU AUA
CAU AUG Met
AAC GUU Val
GAC GUC
UAC GUA
CAC GUG
AGA UCU Ser
GGA UCC
UGA UCA
CGA UCG
ACU AGU Ser
GCU AGC
AGG CCU Pro
GGG CCC
UGG CCA
CGG CCG
AGU ACU Thr
GGU ACC
UGU ACA
CGU ACG
AGC GCU Ala
GGC GCC
UGC GCA
CGC GCG
AUA UAU Tyr
GUA UAC
UUA UAA stop
CUA UAG
AUG CAU His
GUG CAC
UUG CAA Gln
CUG CAG
AUU AAU Asn
GUU AAC
UUU AAA Lys
CUU AAG
AUC GAU Asp
GUC GAC
UUC GAA Glu
CUC GAG
ACA UGU Cys
GCA UGC
UCA UGA stop
CCA UGG Trp
ACG CGU Arg
GCG CGC
UCG CGA
CCG CGG
UCU AGA Arg
CCU AGG
ACC GGU Gly
GCC GGC
UCC GGA
CCC GGG
tRNA gene occurence frequency
0,03350
0,03050
0,02750
0,02450
0,02150
0,01850
0,01550
0,01250
0,00950
0,00650
0,00350
0,00050
A34 clearance in 2-box tRNA sets & Gly (4-box)
3′ 5′
36 35 34
– – A
G34 clearance in 3- and 4-box tRNA sets
3′ 5′
36 35 34
– – G

Figure S10

a

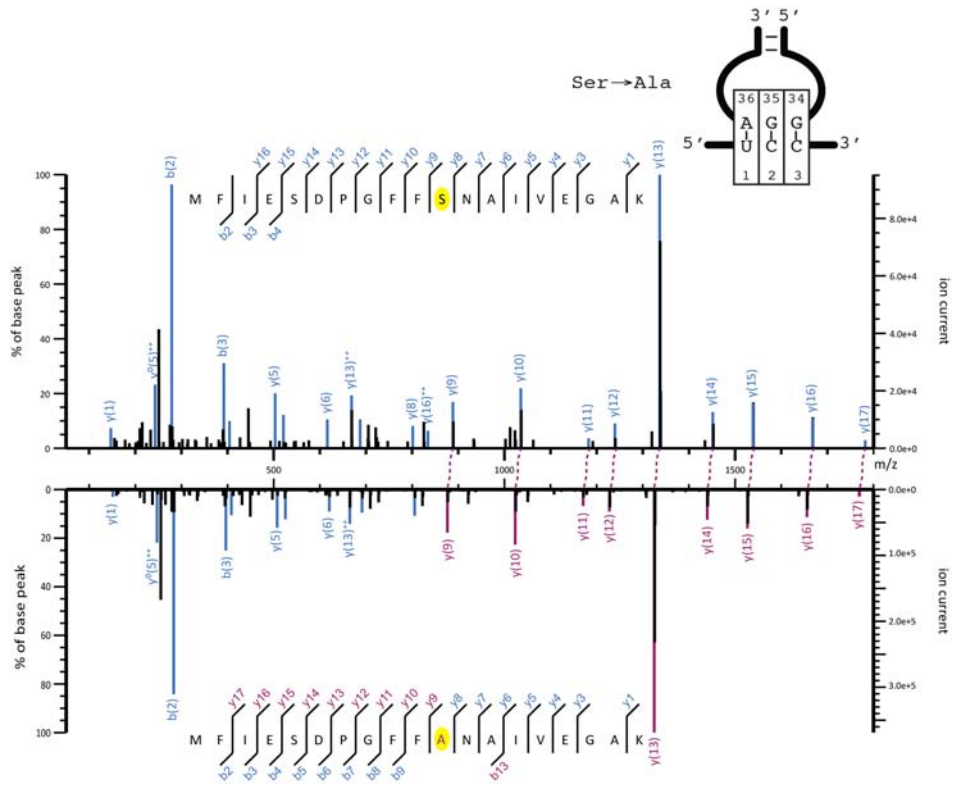

b